581445

Sandia National Laboratories
Waste Isolation Pilot Plant

GEOC-23-10 Milestone Report

Implementation of Geochemistry Conceptual Models

Task 4.4.2.2.1

Author:	Signature on File Patrick Brady, Org. 8880	*04/03/2024* Date
Author:	Signature on File Paul Domski, Org. 8882	*04/03/2024* Date
Author:	Signature on File Isaac Foli, Org. 8882	*04/03/2024* Date
Author:	Jay Jang Jay Jang, Org. 8882	4/3/2024 Date
Author:	Signature on File Ania Pavitt, Org. 8882	*04/03/2024* Date
Author:	Tim Platte Tim Platte, Org. 8882	04/03/2024 Date

Technical Reviewer:	Signature on File Carlos Jove-Colon, Org. 8842	*04/03/2024* Date
QA Reviewer:	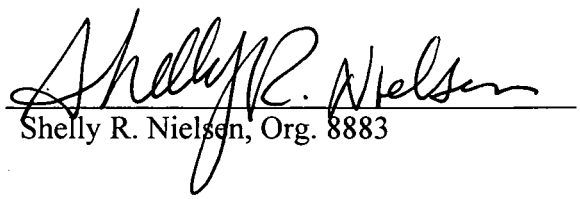 Shelly R. Nielsen, Org. 8883	4-3-2024 Date
Management Reviewer:	Signature on File Chammi Miller, Org. 8882	*04/03/2024* Date

Information Only

GEOC-23-10 Milestone Report
Implementation of Geochemistry Conceptual Models

Information Only

TABLE OF CONTENTS

GEOCHEM-1.0 INTRODUCTION 8

GEOCHEM-2.0 CHEMISTRY-RELATED CONCEPTUAL MODELS 9
- GEOCHEM-2.1 Background 9
- GEOCHEM-2.2 Chemical Conditions 10
- GEOCHEM-2.3 Gas Generation 10
- GEOCHEM-2.4 Dissolved Actinide Source Term 11
- GEOCHEM-2.5 Colloidal Actinide Source Term 11
- GEOCHEM-2.6 Transport of Dissolved Actinides in the Culebra 12
- GEOCHEM-2.7 Chemistry-Related Conceptual Model Conservatisms and Uncertainties 12

GEOCHEM-3.0 CHEMICAL CONDITIONS 14
- GEOCHEM-3.1 Brine Chemistry 14
- GEOCHEM-3.2 The Salado Formation Mineralogy 15
- GEOCHEM-3.3 Calcite Precipitation 16
- GEOCHEM-3.4 The MgO Engineered Barrier 16
- GEOCHEM-3.5 Phase 5 Precipitation 16
- GEOCHEM-3.6 The Waste Container Materials 17
- GEOCHEM-3.7 Iron and Lead Reactants 17
- GEOCHEM-3.8 The Cement Budget 18
- GEOCHEM-3.9 Scaling of Solids 18
- GEOCHEM-3.10 Parameterization of the Chemical Conditions Process Model 18
  - GEOCHEM-3.10.1 The Lead System 19
  - GEOCHEM-3.10.2 The Iron System 20
  - GEOCHEM-3.10.3 Magnesium Model 22
  - GEOCHEM-3.10.4 Earlandite Solubility Product 22

GEOCHEM-4.0 DISSOLVED ACTINIDE SOURCE TERM PROCESS MODEL 23
- GEOCHEM-4.1 The An(III) Model 23
- GEOCHEM-4.2 Comparison of An(III) Models 23
- GEOCHEM-4.3 The Neck et al. (2009) An(III) Model 24
- GEOCHEM-4.4 The Oakes et al. (2021) An(III) Model 25
- GEOCHEM-4.5 Comparison the WIPP, Neck, and Oakes Models for An(III) Solubility 27

GEOCHEM-5.0 DISSOLVED ACTINIDE SOURCE TERM QUANTIFICATION OF UNCERTAINTY SUMMARY 29
- GEOCHEM-5.1 Literature Screening Criteria for Actinide Uncertainty Analysis 29
- GEOCHEM-5.2 Literature Screening 30
- GEOCHEM-5.3 An(IV) Actinide Uncertainty Analysis 30
- GEOCHEM-5.4 An(III) Actinide Uncertainty Analysis 32
- GEOCHEM-5.5 Conclusions of the Actinide Uncertainty Analysis 34

Information Only

GEOCHEM-6.0 GAS GENERATION AND METAL CORROSION 35
GEOCHEM-6.1 Parameterization Uncertainties 35
GEOCHEM-6.1.1 Corrosion Rates 35
GEOCHEM-6.1.2 Corrosion Products 36
GEOCHEM-6.1.3 Gas Generation 37
GEOCHEM-6.1.4 Other Uncertainties 37
GEOCHEM-6.2 Expected Repository Conditions 38
GEOCHEM-6.3 Corrosion Effects on Actinides 39

GEOCHEM-7.0 COLLOIDS 40
GEOCHEM-7.1 Implementation of Colloidal Actinides in PA 40
GEOCHEM-7.2 Changes Since CRA-2019 43
GEOCHEM-7.2.1 Mineral Fragment Colloids 43
GEOCHEM-7.2.2 Intrinsic Colloids 43
GEOCHEM-7.2.3 Humic Substance Colloids 43
GEOCHEM-7.2.4 Microbial Colloids 44

GEOCHEM-8.0 REFERENCES 45

GEOCHEM-9.0 APPENDIX 55
GEOCHEM-9.1 Comparison of Amendments in Appendix GEOCHEM-2019 towards GEOC-23-10 55
GEOCHEM-9.2 Chammi Miller Appendix Geochem 2024 outline 57

Information Only

LIST OF TABLES

Table GEOCHEM 1: Input brine compositions, TDS, and densities used for the Baseline Solubility simulations.....15
Table GEOCHEM 2: Non-radiologic waste Packaging Components.....17
Table GEOCHEM 3: Solubility Products and Aqueous Dissociation Constants for Reactions with Lead that are included in DATA0.FM6.....19
Table GEOCHEM 4: Pitzer Interaction Parameters for the Lead system that are included in DATA0.FM6.....20
Table GEOCHEM 5: Equilibrium Constants for Reactions with Iron that are included in DATA0.FM6.....20
Table GEOCHEM 6: Pitzer Interaction Coefficients (Cation-Anion Interactions) for Ions Containing Iron that are included in DATA0.FM6.....21
Table GEOCHEM 7: Pitzer Interaction Coefficients (Cation-Cation Interactions) for Ions Containing Iron that are included in DATA0.FM6.....21
Table GEOCHEM 8: Pitzer Interaction Coefficients (Cation-Cation-Anion Interactions) for Ions Containing Iron that are included in DATA0.FM6.....22
Table GEOCHEM 9: Reactions and log K values at 25 °C and I = 0 used for the Mg-Oxalate system.....22
Table GEOCHEM 10: Solubility constant of Earlandite ($Ca_3(Citrate)_2 \cdot 4H_2O$) to be implemented in DATA0.FM6.....22
Table GEOCHEM 11: Recommendation of new Pitzer parameters for the $Nd(OH)_3(s)$ - $MgCl_2$ - H_2O system. Note: Nd(III) is an analog for Am(III).....23
Table GEOCHEM 12: Am – Cl aqueous species concentrations.....27
Table GEOCHEM 13: Statistical Properties of the Distribution of D = log10(Sm) – log10(Sp) for Th(IV) for the RPPCR compared with the CRA-2019 DPA data (Domski, 2019b).....32
Table GEOCHEM 14: Statistical Properties of the Distribution of D = log10(Sm) – log10(Sp) for An(III) for RPPCR compared with the CRA-2019 DPA data (Domski, 2019b).....34
Table GEOCHEM 15: WIPP Colloid Model Parameter Summary.....40
Table GEOCHEM 16: WIPP Colloid Parameter Values Estimated for Use in CRA-2019 (DOE, 2019b) and the next CRA.....42
Table GEOCHEM 17: Comparison GEOCHEM-2019 with SOTERM-2019.....56

Information Only

LIST OF FIGURES

Figure GEOCHEM 1: From (Domski, 2022) Figure 1D and Figure 2A, for 5.0 M NaCl and 0.25 M $MgCl_2$ and $MgCl_2$ solutions, showing the measured data as symbols and EQ3/6 simulated data as lines. 25
Figure GEOCHEM 2: Comparison of Konnecke et al. (1997), Oakes et al. (2021) and EQ3/6 results of SNL. Note that on the figure of Oakes et al. (2021) the axes are reversed from that of the original work by Konnecke. 26
Figure GEOCHEM 3: An(III) models compared to measured An(III) data (see below for model descriptions. 28
Figure GEOCHEM 4: Histogram for the RPPCR of the difference D = log10 Sm – log10 Sp for Th(IV). 31
Figure GEOCHEM 5: CDF plot for the RPPCR of the difference D = log10 Sm – log10 Sp for Th(IV). 31
Figure GEOCHEM 6: Histogram for the RPPCR of the difference D = log10 Sm – log10 Sp Am(III). 33
Figure GEOCHEM 7: CDF plot for the RPPCR of the difference D = log10 Sm – log10 Sp for Am(III). 33
Figure GEOCHEM 8: Variance in the elemental composition of the different types of steel and grades used in the WIPP. Different elements are denoted by different colors. Square markers correspond to the right y-axis, all other markers use the left y-axis. X-markers represent elements whose composition does not vary greatly; triangle markers represent elements that are in less than 10% of the steel listed. 36
Figure GEOCHEM 9: Evolution of changes between GEOCHEM-2019 to GEOC-23-10..... 55

Information Only

ACRONYMS AND ABBREVIATIONS

%	percent
α_i	constant in Pitzer model, i = 1 or 2
a_i	activity of a chemical species
atm	atmosphere
β	(apparent) stability constant, or beta particle
$\beta^{(0)}$, $\beta^{(1)}$, $\beta^{(2)}$	parameters within Pitzer's 2nd virial coefficient term B_{MX}
b	constant in f^{γ}, f^{ϕ}
B_{fc}	parameter to account for the uncertainty in microbial gas generation
C^{ϕ}_{MX}, C_{MX}	Pitzer parameter for osmotic and activity coefficient functions representing interaction between cation M and anion X
CAPHUM	maximum (cap) actinide concentration associated with mobile humic colloids
CAPMIC	maximum actinide concentration that could be associated with microbes
CCA	Compliance Certification Application
CCDF	complementary cumulative distribution functions
CDF	cumulative distribution function
CFR	Code of Federal Regulations
c_i	aqueous species concentrations at equilibrium
CONCINT	actinide concentration associated with mobile actinide intrinsic colloids
CONCMIN	actinide concentration associated with mobile mineral fragment colloids
CPR	cellulosic, plastic, and rubber materials
cr	crystalline phase
CRA	Compliance Recertification Application
DBR	direct brine releases
D_C	mass concentration of cellulosics; (material mass)/(disposal volume)
D_{HM}	mass concentration of MgO; (hydromagnesite mass)/(disposal volume)
D_m	mass concentration of MgO; (MgO mass)/(disposal volume)
DOE	U.S. Department of Energy
DRZ	disturbed rock zone
DPA	Deferred Performance Assessment
D_s	surface area concentration of steel; (surface area steel)/(disposal volume)
EDTA	ethylenediaminetetraacetic acid
E_h	oxidation-reduction (redox) potential under specific conditions
EPA	U.S. Environmental Protection Agency
EQ3/6	software program for geochemical modeling of aqueous systems
EQ3NR	aqueous solution speciation-solubility modeling code
ERDA-6	Energy Research and Development Administration Well 6
eV	electron volt
F	Fahrenheit or function containing f^{γ} and ionic strength derivatives of Pitzer model 2nd virial coefficient terms
f^{γ}, f^{ϕ}	Debye-Hückel function for activity and osmotic coefficients, respectively
f_{CO_2}	fugacity of carbon dioxide

Information Only

F_{NO3}, F_{SO4}	fraction of carbon consumed through microbial denitrification or sulfate reduction
ft	foot/feet
g	gamma radiation or activity coefficient
G	molecular yield in molecules/100 eV of absorbed ionizing radiation or Gibbs free energy (G^{xs} is excess or non-ideal contribution to Gibbs free energy)
g	gaseous, or gram, or gravity of Earth
GWB	generic weep brine
h	hours
I	ionic strength
IUPAC	International Union of Pure and Applied Chemists
K	degree Kelvin or stability constant
K_d	distribution coefficient
kg	kilogram
K_s	solubility constant, K_{sp}
ksp	solubility product constant
L	liter
LANL	Los Alamos National Laboratory
log	logarithm
µ, or µm	micrometer, micron
M	mole per liter or molecular mass of subscripted species
m	meter, molal
m^2	square meter
m^3	cubic meter
meq	milliequivalents
mg	milligram
min	minimum
mL	Milliliters
mM	millimole per liter
mol	mole
MPa	megapascal
N	degree of polymerization number
n	neutron, number, or number of moles
NEA	Nuclear Energy Agency
nm	Nanometer
ϕ	osmotic coefficient
P	pressure
PA	Performance Assessment
PABC	Performance Assessment Baseline Calculation
PAIR	Performance Assessment Inventory Report
PAVT	Performance Assessment Verification Test
pC_{H+} or pcH	negative logarithm of H^+ concentration in moles per liter
pH	negative logarithm of H^+ activity
PHUMCIM	proportionality constant for the actinide concentration associated with mobile humic colloids, in Castile brine

Information Only

PHUMSIM	proportionality constant for the actinide concentration associated with mobile humic colloids, in Salado brine
pmH	negative logarithm of H^+ concentration in molal
ppm	parts per million
PROPMIC	proportionality constant describing the bioassociation of actinides with mobile microorganisms
q_r	gas (q_{rg}), brine (q_{rb}) generation rates by corrosion, sulfidation, microbes, MgO, or hydromagnesite – trailing subscripted c, s, m, h, & hc, respectively
ρ	density
R	gas constant, 8.31446 J/(mol·K)
R_c	corrosion rate in either inundated (R_{ci}) or humid air (R_{ch})
redox	oxidation-reduction
RH	relative humidity
R_h	MgO hydration rate in either inundated (R_{hi}) or humid air (R_{hh})
R_{hc}	rate of conversion of hydromagnesite to magnesite
R_m	biodegradation rate in either inundated (R_{mi}) or humid air (R_{mh})
RPPCR	Replacement Panels Planned Change Request
s	solid or second
S_b	brine saturation
SEM	Scanning Electron Microscope
SNL	Sandia National Laboratories
SOTERM	Actinide Chemistry Source Term (WIPP)
σ	standard deviation of a normal distribution
T	temperature
TDS	total dissolved solids
TIC	total inorganic carbon
TRU	Transuranic
TSD	Technical Support Document
V	volt, vanadium, or volume
WIPP	Waste Isolation Pilot Plant
X	stoichiometric coefficient for gas generation by corrosion, sulfidation, microbes, MgO hydration, or hydromagnesite conversion– trailing subscripted c, s, m, h, & hc, respectively
Xm	stoichiometric coefficient for gas generation by microbes
XRD	X-ray diffraction
yr	year
Z	sum of products for each species' molality multiplied by absolute value of its valence charge
ZVI	zero valent iron
z_s	valence charge of solute species s

Information Only

GEOCHEM-1.0 Introduction

The Waste Isolation Pilot Plant (WIPP) is a U.S. Department of Energy (DOE) facility for the permanent disposal of transuranic (TRU) waste. The WIPP must be recertified every five years from the date of determination of completeness by the U.S. Environmental Protection Agency (EPA). The EPA's assessment of the WIPP's ability to comply with containment requirements specified in 40 Code of Federal Regulations (CFR) 191.13 is based, in part, on performance assessment (PA) calculations.

This Milestone Report is a summary of the updates to the process models which support the Chemical Conditions, Dissolved Actinide Source Term, Colloidal Actinide Source Term, and Gas Generation conceptual models since the 2019 Compliance Recertification Application Deferred Performance Assessment (CRA-2019 DPA). These supporting process models provide the chemical environment of the repository and the total dissolved actinide (+III, +IV, and +V)[1] concentrations as inputs to PA. There have been no changes to the conceptual models. This document is not a compliance document. The intention of this document is to highlight suggested changes/updates to CRA-2019 process models and align with APPENDIX SOTERM.

WIPP PA calculations are carried out by the DOE using linked computer models that calculate the probabilities of cumulative radionuclide releases from the disposal system during the 10,000 years following closure. These computer models and the parameters included in the calculations are based on conceptual models that describe the expected performance of the disposal system.

The WIPP chemistry-related conceptual models include: Gas Generation, Chemical Conditions, Dissolved Actinide Source Term, Colloidal Actinide Source Term, Transport of Dissolved Actinides in the Culebra, and Transport of Colloidal Actinides in the Culebra. Since the CRA-2019 DPA the DOE has continued studying processes related to WIPP repository chemistry. Consequently, additional information has become available to the chemical conditions process model and the dissolved actinide source term models, including actinide solubilities, the lead and iron thermodynamic models, model assumptions with regard to carbonate phase precipitation and magnesium hydroxy-chloride phases, the scaling of reactants from inventory scale to that used in the model, and the criteria used to screen experimental studies used for the actinide uncertainty analysis. The purpose of this Milestone Report is to document the updates to the process models, process-model parameterization, and quantification of uncertainty.

[1] The An(VI) concentration is set to the constant value of 1×10^{-3} M, see Section 2.2.8 of Brush and Domski (2012) for a detailed discussion of this topic.

Information Only

GEOCHEM-2.0 Chemistry-Related Conceptual Models

GEOCHEM-2.1 Background

Cuttings, cavings, direct brine releases (DBRs), and spallings are calculated to be the most significant pathways for release of radioactive material to the land surface; contributions to total releases from Culebra transport are much less significant to performance (DOE, 2019b). Accurately predicting actinide concentrations in the Salado, DBR fluids, and the Culebra are an important component of the chemistry-related conceptual models. The models are: Chemical Conditions, Gas Generation, Dissolved Actinide Source Term, Colloidal Actinide Source Term, Transport of Dissolved Actinides in the Culebra, and Transport of Colloidal Actinides in the Culebra. Each makes qualitative assumptions about underlying processes. The models and their assumptions were peer reviewed in 1996 (Wilson et al., 1996), and reviewed by the EPA in 2008 (EPA, 2008) and 2019 (EPA, 2019).

The chemistry-related conceptual models are coupled to the mineralogy of the Salado host rock and the composition of Salado and Castille brines (DOE, 2019a). The models also depend upon the composition of the waste – actinide-contaminated residue from laboratory operations (glassware, paper goods, laboratory analysis byproducts) and materials from demolition and clean-up of TRU-contaminated facilities (DOE, 2019a); and diluted surplus Pu. The waste includes cellulosic, plastic, and rubber (CPR) materials, microbial breakdown of which produces humic acid colloidal material and CO_2. MgO backfill will limit disposal area CO_2 levels (DOE, 2014). Microbes, actinide-complexing humic acids, actinide-bearing mineral fragments, and intrinsic colloids might mobilize actinides above their baseline solubilities (DOE, 1996b).

The Chemical Conditions conceptual model identifies the factors controlling the composition (f_{CO2}, pcH, I, and bulk aqueous species concentrations at equilibrium (c_i)) of WIPP fluids and is based in part, on the Gas Generation conceptual model which establishes controls over CO_2, O_2, H_2, and H_2S levels by a combination of CPR breakdown and metal corrosion coupled to sulfate reduction and denitrification, radiolysis, and MgO reaction with CO_2. The Dissolved Actinide Source Term, Colloidal Source Term, and Culebra Dissolved and Colloid Actinide Transport models use the boundary conditions set by the Chemical Conditions model (DOE, 2019a).

The Colloidal Source Term conceptual model describes generation and stabilization of actinide-associated colloids and humic acids in DBR fluids and fluids going into the Culebra and marker beds. The chemistry-related portion of the Transport of Dissolved and Colloidal Actinides in the Culebra conceptual model describes sorption of dissolved actinides onto dolomite in the Culebra.

Information Only

GEOCHEM-2.2 Chemical Conditions

The Chemical Conditions conceptual model estimates a range in bulk compositions of disposal area brines by making the following simplifying assumptions (DOE, 2019a):

- Fixed compositions of Salado and Castile Formation minerals including halite and anhydrite,
- Fixed compositions of Salado and Castile brines before contacting the MgO and waste,
- That the disposal area behaves as a well-mixed batch reactor at reversible equilibrium, except that Fe metal corrosion and CPR degradation are kinetically controlled, because they are out of equilibrium,
- Reducing conditions in the long-term because of Fe metal corrosion; available oxygen will be consumed within 100 years of closure,
- Low CO_2 fugacities controlled by $Mg(OH)_2$ – hydromagnesite equilibria,
- Ambient temperatures are expected to remain close to 27°C for the disposal time period.

GEOCHEM-2.3 Gas Generation

The Gas Generation conceptual model uses an average stoichiometry model for predicting gas generation by anoxic corrosion of steels and microbial degradation of CPR, and radiolysis, and makes the following simplifying assumptions (DOE, 2019a):

- Gas generation can take place in all waste areas,
- Corrosion reactions between brine and iron waste containers can produce H_2; reactions between microbes, brine, and CPR materials will primarily yield CO_2, H_2S, and water (and N_2 from denitrification),
- CO_2 produced by microbial CPR degradation will be consumed by $Mg(OH)_2$, with partial pressures of CO_2 maintained by hydromagnesite equilibria,
- Iron corrosion will occur anoxically because anoxic conditions will prevail over long term,
- Radiolysis of water in brine will occur,
- Oxygen produced by radiolysis will be consumed by metal corrosion,
- No passivation of anoxic corrosion of steel by microbially-produced CO_2 and H_2S.

The Gas Generation Conceptual Model considers corrosion of non-ferrous metals, for example, lead and aluminum, but screens them out on the basis of low consequence (DOE, 2019a).

Information Only

GEOCHEM-2.4 Dissolved Actinide Source Term

The Dissolved Actinide Source Term conceptual model uses the Chemical Conditions bulk fluid compositional bounds to predict actinide speciation and solubilities with the geochemical reaction path code EQ3/6. The Dissolved Actinide Source Term conceptual model makes the following simplifying assumptions (DOE, 2019a)

- Spontaneously mixed brine and waste,
- Salado and Castile brine compositions bracket possible brine chemistries,
- Equilibria between actinide solids and dissolved actinides,
- Solubility control of Am(III), Cm(III), and Pu(III) by $AmOHCO_3$ are modeled using +3 oxidation solid phases,
- Solubility control of Th(IV) by ThO_2(am); Pu(IV) are modeled using oxidation-state analogues,
- The solubilities of neptunium and uranium in the +IV oxidation state are modeled using the solubility of thorium(IV),
- The solubility of neptunium(V) is based on experimental data for neptunium(V),
- An an upper-limit solubility of 1 × 10-3 M is assumed for U(VI),
- Redox in the repository is assumed to be strongly influenced by steel corrosion kinetics. The steel corrosion analysis is described in Appendix-PA-2019 (DOE, 2019b, Section PA-1.1.5). WIPP system redox is discussed in SOTERM-2019 (DOE 2019d, Section-6.1.1).
- Equilibrium between anhydrite, halite, MgO, and the brine,
- No adsorption of actinides onto immobile minerals or waste.

GEOCHEM-2.5 Colloidal Actinide Source Term

The Colloidal Actinide Source Term considers how microbes, humic acids, mineral fragment, and intrinsic colloids can be mobilized by brines, and at what levels.

Potential sources of humic acids and microbes include organic and soil-bearing wastes, organic waste degradation, as well as naturally occurring organic colloids in Salado and Castile brines. Humic colloids associate with actinides by complexation with their carboxylic and hydroxyl functional groups. Microbes can incorporate actinides both externally on their surfaces and internally into their cells.

Mineral fragment colloids might be released from the host rock by changes in fluid chemistry or physical disruption, by corrosion of the waste solids, by degradation of cement, and by drilling mud. Mineral fragment colloids incorporate actinides by sorption or surface co-precipitation. Intrinsic colloids can form from dissolved actinides once the actinides reach saturation. Intrinsic colloids, if they form, are largely composed of a single actinide, and are not expected to sorb other actinides.

The Colloidal Actinide Source Term conceptual model makes the following simplifying assumptions (DOE, 1996b):

Information Only

- Once suspended, mobile colloid concentrations are fixed in the disposal area; no new colloids form, no colloids leave solution through adsorption, settling, or filtration,
- Each of the individual actinides fills the entire total site capacity of mineral fragment colloids provided sufficient actinide inventory,
- No competition between other ions and actinides on mineral fragment colloids,
- No actinide sorption onto intrinsic colloids,
- Maximum intrinsic colloid concentrations are assumed to be equal to their respective calculated solubilities.

GEOCHEM-2.6 Transport of Dissolved Actinides in the Culebra

Actinides introduced into the Culebra by brine flowing up a borehole or by brine flowing up the shaft can advect through fracture porosity, diffuse into the matrix, and/or sorb onto Culebra minerals. The Transport of Dissolved Actinides in the Culebra conceptual model assumes only sorption onto Culebra dolomite and makes the following simplifying assumptions:

- Homogeneous Culebra lithology,
- No incorporation of actinides into immobile solids,
- Sorption of actinides onto Culebra Dolomite obeys a linear partition relationship (K_d),
- No actinide sorption onto Culebra clays.

GEOCHEM-2.7 Chemistry-Related Conceptual Model Conservatisms and Uncertainties

The main simplifying assumptions in the Chemistry-Related Conceptual Models are:

- The disposal area behaves as a well-mixed batch reactor at equilibrium, except for redox which is strongly influenced by steel corrosion kinetics (see Appendix-PA-2019 (DOE, 2019b, Section PA-1.1.5) and SOTERM-2019 (2019d, Section SOTERM-6.1.1)),
- No consideration of actinide interaction with waste phosphate,
- No sorption of humic acids or microbes by MgO,
- No sorption of actinides in the disposal area.

Assuming the disposal area is a well-mixed batch reactor is unavoidable, because the complex temporal and spatial distribution of reactants and products in the disposal area cannot be predicted at present. The other assumptions listed above are conservative, that is, they bias the modeled actinide concentrations towards higher values than what would be predicted had the particular effect been included.

Release of waste phosphate might cause formation of low solubility actinide phosphate minerals and the formation of actinide-sorbing hydroxylapatite. Appendix-SOTERM-2019 notes that "the sorption of colloidal actinides onto fixed substrates and their filtration in low-porosity media will also reduce the mobile colloidal actinide source term, but no credit is currently being taken for this potentially significant reduction in colloidal concentrations" (DOE, 2019d).

Information Only

The current conceptual model assumes that humic acid levels remain fixed, yet Wall and Matthews (Wall & Mathews, 2005) measured substantial sorption of humic acids from WIPP brines by MgO backfill. Sorption of microbes onto hydrated MgO is not in the conceptual model, yet hydrated MgO should remove microbial colloids from WIPP the same way $Mg(OH)_2$ is used to remove microbes (microalgae) from wastewater e.g. (Folkman & Wachs, 1973; Smith & Davis, 2012; Young et al., 2021); positively charged $Mg(OH)_2$ surfaces sorbing microbes through microbe surface carboxylate and phenolate groups.

Probably the most conservative of the Chemistry-Related Conceptual Model assumptions is that no actinides sorb onto immobile minerals, or waste in the disturbed rock zone (DRZ) and disposal zone. Regarding actinide sorption to waste, Appendix-SOTERM-2019, states, "This is a large conservatism built into the model that has a large impact on inventory-limited actinides (essentially Am, Cm, Ac, and Np). The conceptual model recognizes that there will be many phases within the WIPP that will be sorptive and in some cases highly sorptive. Iron minerals are the most important example of this. Lead oxides, phases of other metals, and microbes/biomass provide highly sorptive surfaces that in reality enhance immobilization" (DOE, 2019d). Other sorptive components in the waste include cements, Al corrosion products, and potentially hydroxylapatite formed after release of waste phosphate. The DRZ itself will sorb actinides; (Dosch & Lynch, 1978) measured substantial sorptive uptake of actinides by Salado halite, anhydrite, and clays, and stated that, "the halite in the vicinity of the repository can serve as a barrier to actinide migration".

Information Only

GEOCHEM-3.0 Chemical Conditions

The chemical conditions model is implemented, in part, by the following four models: 1) The MgO hydration model, 2) the iron corrosion model, 3) the CPR degradation model, and 4) an equilibrium-chemical model. The gas-generation effects of the MgO hydration, Fe corrosion, and CPR degradation models are included in PA, and the equilibrium chemical model is implemented in EQ3/6 version 8.0a[2] (Wolery & Jarek, 2003; Wolery et al., 2011). The chemical-equilibrium model simulates the near-field chemical conditions of the repository and provides the expected equilibrium chemical conditions and actinide solubility values.

The computational implementation of the chemical-equilibrium model entails the use of the geochemical modeling software EQ3/6, to simulate the interaction of WIPP brines (GWB and ERDA-6) with Salado mineralogy, MgO engineered barrier, waste package materials, and waste components. The chemical equilibrium model combines parts of the chemical conditions and the dissolved actinide source term process model in a single computational model to provide the near-field chemical conditions and the total dissolved actinide (+III, +IV, and +V) solubility values for WIPP PA calculations. This combined chemical-equilibrium model is known as the "baseline solubility model."

The RPPCR baseline solubility model differs from the 2019 Compliance Recertification Application Deferred Performance Assessment (CRA-2019 DPA) baseline solubility model (Domski & Sisk-Scott, 2019) in four ways: 1) The updated WIPP thermodynamic database DATA0.FM6 (Domski, 2023c) was used rather than DATA0.FM4; 2) the RPPCR is based on a new 19-panel repository geometry, which increased the minimum brine volume required for a direct brine release (King, 2021) which in turn affects the scaling of the reactants used in the solubility model; 3) a new inventory was issued for the RPPCR (Van Soest, 2022) which provides updated inventories for the reactants used in the solubility model; 4) model assumptions were updated with regard to calcite precipitation, phase-5 precipitation, and scaling of the reactants.

GEOCHEM-3.1 Brine Chemistry

WIPP PA predicts that: (1) intergranular brine could seep into the disposal rooms from the disturbed rock zone (DRZ) in the surrounding Salado Formation (Fm.) after the panels are filled and closed, (2) brine could flow down into the repository from overlying formations if future exploratory drilling inadvertently penetrates the repository, and (3) brine could flow up into the repository from reservoirs in the underlying Castile Fm., if drilling penetrates both the repository and a Castile brine reservoir. As a simplifying assumption, PA assumes that in the second case listed above brine from formations above the repository would react with Salado minerals to an

[2] The CRA-2019 DPA APPENDIX GEOCHEM, Section 3.2 provides an exhaustive discussion of the history of the computer codes used for implementation of this model that will not be repeated here.

Information Only

extent sufficient to produce a composition identical to that of intergranular Salado brines. These assumptions and predictions are described in detail in (DOE, 1996a, 2004).

The unreacted ERDA-6 (Popielak et al., 1983), and GWB (Krumhansl et al., 1991; Snider, 2003) brine compositions that were used as input for the EQ3NR code are listed in Table GEOCHEM 1.

Table GEOCHEM 1: Input brine compositions, TDS, and densities used for the Baseline Solubility simulations.

	ERDA-6	GWB	
Na^+	4.87	3.53	Molarity
K^+	9.70E-02	4.67E-01	Molarity
Mg^{2+}	1.90E-02	1.02	Molarity
Ca^{2+}	1.20E-02	1.40E-02	Molarity
Cl^-	4.80	5.86	Molarity
HCO_3^-	1.60E-02	1.60E-02	Molarity
$SO4^{2-}$	1.70E-01	1.77E-01	Molarity
$B(OH)_4^-$	6.30E-02	1.58E-01	Molarity
Br^-	1.10E-02	2.66E-02	Molarity
H^+	7.00	7.00	pmH
TDS[A]	313167.7	368202.9	mg/L
Density[A]	1.20138	1.2366	g/cm^3

A – The total dissolved solids (TDS) and density values in Table 3 are not used in the EQ3NR input files because they do not account for the organic ligands.

The initial value of the total inorganic carbon (TIC), represented as HCO_3^-, for both brines was set at 16 mM for this step because: (1) (Popielak et al., 1983) reported that the average TIC content of ERDA-6 was 16 mM, (2) the initial TIC of GWB was not determined, hence (3) it was assumed that the initial TIC content of GWB was equal to that of ERDA-6 (Brush et al., 2012). The initial value of the TIC did not affect the values of the TIC predicted during the rest of the calculations. The pmH for both brines is set to 7.0.

GEOCHEM-3.2 The Salado Formation Mineralogy

The mineralogy of the Salado Formation in the WIPP stratigraphic horizon was studied by (Stein, 1985). The results of Stein's analysis were an accounting of *"...quantities, distribution, and mineralogical species of the non-NaCl components of halite and anhydrites in the immediate vicinity (e.g., within 100 vertical feet) of the WIPP facility horizon".*

To calculate the quantities of halite and anhydrite for the conservatively large DRZ currently implemented in WIPP PA it was assumed that the DRZ is comprised of 90 wt % halite and 10 wt % anhydrite. This mineralogical composition is similar to Brush's (1990) interpretation of the results of Stein's mineralogical analysis of the Salado Fm. at or near the stratigraphic horizon of

Information Only

the repository: (Brush, 1990) concluded that, for use in geochemical modeling, the Salado consists of 93.2 wt % halite and 1.7 wt % each of anhydrite, gypsum ($CaSO_4 \cdot 2H_2O$), magnesite ($MgCO_3$), and polyhalite ($K_2MgCa_2(SO_4)_4 2H_2O$). However, it was assumed for this analysis that the Salado contains 90 wt % halite and 10 wt % anhydrite because the conceptual models for WIPP near-field chemistry used in PA include only halite and anhydrite ((Associates), 2008).

GEOCHEM-3.3 Calcite Precipitation

For the CRA-2019 DPA Domski and Sisk-Scott (Domski & Sisk-Scott, 2019) allowed calcite to precipitate because its saturation index, in some cases, was in excess of 1.5 log units above saturation. However, as documented by (Domski, 2023a) for the Replacement Panels Planned Change Request (RPPCR), calcite precipitation in complex brines may be inhibited by the presence of ions such as Mg^{2+} and Fe^{2+} (Brush et al., 2006; Katz et al., 1993; Zhu et al., 2018). It has been observed that in conditions where calcite inhibitors may be present that a disordered, more soluble form of $CaCO_3$ may precipitate such as non-biogenic aragonite. Jaohari et al. (Jaouhari et al., 2000) observed aragonite to precipitate from synthetic seawater on an iron substrate in the presence of Mg^{2+} ions – two conditions that could be expected at WIPP. For the RPPCR baseline solubility calculations, calcite was suppressed such that it may reach over saturation to the point where aragonite becomes saturated and precipitates. The EPA had identified calcite formation as Issue 6 in the letter by Peake (Peake, 2022), and Domski (Domski, 2023a) for the RPPCR provided a more reasoned argument of $CaCO_3$ precipitation than Domski and Sisk-Scott (Domski & Sisk-Scott, 2019).

GEOCHEM-3.4 The MgO Engineered Barrier

The purpose of the MgO engineered barrier is to facilitate a chemical environment of low carbon dioxide fugacity and moderately high pH (~9) - conditions which are conducive to low actinide solubility. The hydration and carbonation products of MgO are brucite ($Mg(OH)_2$) and hydromagnesite ($Mg_5(CO_3)_4(OH)_2 \cdot 4H_2O$), respectively, which, together, form a buffer reaction that moderates the pH and $f_{CO_2}(g)$ in the range of low actinide solubility. See (Brush et al., 2012) for a detailed discussion of the MgO buffer reactions.

GEOCHEM-3.5 Phase 5 Precipitation

Domski and Nemer (Domski & Nemer, 2023a) examined the occurrence and solubility of the Sorel cement phases phase-3 ($Mg_2Cl(OH)_3.4H_2O$) and phase-5 ($Mg_3Cl(OH)_5.4H_2O$) under expected WIPP conditions in effort to address the EPA's Issue 7 (Peake, 2022). Issue 7 is concerned with the examination of the phase-5 solubility constant, and whether the low value used in the WIPP model led to significant phase-5 precipitation and significant water consumption in the CRA-2019 DPA actinide solubility calculations. Domski and Nemer (Domski & Nemer, 2023a) reviewed papers by Altmaier et al. (Altmaier et al., 2003), Pannach et al. (Pannach et al., 2017), Xiong and Lord (Xiong & Lord, 2008), Deng et al. (Deng et al., 2009), and Xiong et al. (Xiong et al., 2010). The results of the literature review concluded that the stability fields of phase-3 and phase-5 are close: evidence (Pannach et al., 2017) suggests that phase-5 is

Information Only

metastable with respect to phase-3 in some brines. Phase-5 formed in GWB and not in ERDA-6 brines, there appears to be sufficient uncertainty in the log K value of phase-5 such that a computational prediction of the stable phase is indeterminate. Based on these conclusions, Domski and Nemer (Domski & Nemer, 2023a) recommend that phase-5 should be suppressed in future calculations of actinide solubility, until evidence suggests otherwise. Phase-5 was not allowed in the next CRA baseline solubility model.

GEOCHEM-3.6 The Waste Container Materials

In Van Soest (Van Soest, 2022) Tables 5-5 and 5-6 provide the masses of the waste package components. The remote handled (RH) and contact handled (CH) mass values for each component were combined, as were the cement totals from Tables 5-5 and 5-6, and the percent of each component was calculated as shown in Table GEOCHEM 2 below.

Table GEOCHEM 2: Non-radiologic waste Packaging Components.

Waste and/or Waste Package Component	Mass %
Iron-based Metal/Alloys	48.76%
CPR	12.34%
Other Inorganic Materials	8.27%
Solidified Inorganic Material	8.13%
Lead	6.82%
Cement	6.71%
Soil	5.21%
Solidified Organic Material	2.54%
Other Metal/Alloys	0.85%
Aluminum-based Metal/Alloys	0.36%
	100.00%

For the RPPCR only the iron-based metal/alloys, CPR, and lead are included in the chemical conditions process model. The mass of cement is compared to the mass of MgO engineered barrier materials to determine if the cement budget exceeds the buffer capacity of the MgO.

GEOCHEM-3.7 Iron and Lead Reactants

Iron and lead comprise a significant fraction of the non-radiologic materials to be stored at WIPP (Table GEOCHEM 2 above). For RPPCR the iron and lead reactants used in the baseline solubility model were different from those used for the CRA-2019 DPA. The lead and iron reactants used for the CRA-2019 DPA calculations, PbO and $Fe(OH)_2$, were replaced with hydrocerussite ($2PbCO_3.Pb(OH)_2(s)$) and hibbingite ($Fe_2Cl(OH)_3$), respectively. See (Domski, 2023a) for a detailed discussion of the iron and lead reactants.

Information Only

GEOCHEM-3.8 The Cement Budget

Cement makes up about 7% of the non-radiological waste to be stored at WIPP (see Table GEOCHEM 2). One of the primary components of cement is the mineral phase Portlandite ($Ca(OH)_2$), which increases the pH of the system via the reaction:

$$Ca(OH)_2 \rightleftharpoons Ca^{2+} + 2\,OH^- \qquad (Eq\ 1)$$

However, in the presence of carbonate portlandite will react to form calcite:

$$Ca(OH)_2 + CO_{2(aq)} \rightleftharpoons CaCO_{3(s)} + H_2O \qquad (Eq\ 2)$$

The formation of calcite from the reaction of portlandite and carbon dioxide neutralizes the two moles hydroxide ion from portlandite and moderates the pH. The only source of carbonate in the WIPP actinide solubility model is the initial concentration in the brines. The CO_2(g) liberated from the degradation of the CPR materials where the carbonate is then sequestered by the mineral phase hydromagnesite, from the conversion of brucite, otherwise the system is closed to carbonate. The addition of portlandite to the WIPP baseline solubility model would increase the demand for carbonate via the conversion of portlandite to calcite with an increased demand on hydromagnesite dissolution, via the reaction:

$$4\,Ca(OH)_2 + Mg_5(CO_3)_4(OH)_2 * 4\,H_2O + 10\,H^+ \rightleftharpoons 4\,CaCO_3 + 5\,Mg^{2+} + 14\,H_2O \quad (Eq\ 3)$$

This reaction, presented for illustrative purposes only, shows that eight moles of hydroxide ion from portlandite dissolution are neutralized for each mole of hydromagnesite that is dissolved, Calcium carbonate forms in a one-to-one mole ratio with portlandite dissolution. Therefore, to neutralize the effect on pH of cement the total moles of portlandite may not exceed 25% of the hydromagnesite in the repository which is assumed to be 50% of the total MgO.

GEOCHEM-3.9 Scaling of Solids

EPA Issue 28 states the moles of reactants should decrease with increasing brine volume, was resolved in the RPPCR (Domski, 2023a) and RPPCR actinide solubility calculations by scaling the reactant masses to the 1x, 2x, 3x, 4x, and 5x volumes. Doing so had no effect on the calculated actinide solubilities, because even when scaled to the highest 5x volume the reactants were still present in excess (Domski, 2023a).

GEOCHEM-3.10 Parameterization of the Chemical Conditions Process Model

Parameterization of the Chemical Conditions process model included updates to the WIPP thermodynamic database. The parameter updates to the thermodynamic database used for CRA-

Information Only

2019 DPA, DATA0.FM4, and its successor, DATA0.FM5, were discarded, and for the current update the DATA0.FM1 database was updated to create DATA0.FM6. By using DATA0.FM1 the EPA issues 5, 8, 11, 29, 30, and 32 outlined in Peake (Peake, 2022) were resolved. All of the information provided in the following sections was taken from (Domski, 2023c), and the reader is referred to that document for more complete information.

For a detailed discussion of the legacy parameters included in DATA0.FM1, and thus, DATA0.FM6, the reader is directed to the CRA-2019 DPA Appendix GEOCHEM Sections 3.3.3 – 3.3.6, note Sections 3.3.7 and 3.3.8 are for the lead and iron systems, respectively, which are included in the following sections.

GEOCHEM-3.10.1 The Lead System

The lead system as presented in (Jang, 2021, 2022, 2023a; Jang & Foil, 2023; Jang et al., 2021) is included in DATA0.FM6, and the reader is directed to these documents for detailed discussion of the parameters. Inclusion of a Pitzer based lead-chloride model in the WIPP database addresses EPA Issue 8 (Peake, 2022) additional Pitzer based lead systems may be added in the future.

This section, Table GEOCHEM 3 and Table GEOCHEM 4, provide the parameters for the lead systems that are included in DATA0.FM6.

Table GEOCHEM 3: Solubility Products and Aqueous Dissociation Constants for Reactions with Lead that are included in DATA0.FM6.

Reaction	log K	Source
Solid Dissolution Reactions		
$PbCl_2(s)$ (Cotunnite) ⇌ $Pb^{2+} + 2Cl^-$	-4.83	(Edwards et al., 1992) and (Jang, 2021)
$PbCO_3(s)$ (Cerussite) + H^+ ⇌ $Pb^{2+} + HCO3^-$	-2.85	(Powell et al., 2009)
$NaPb_2(CO_3)_2(OH)(s)$ (Abellaite) + $3H^+$ ⇌ $Na^+ + 2Pb^{2+} + 2HCO_3^- + H_2O$	2.59	(Jang, 2022)
$2Pb(CO_3)_2.Pb(OH)_2(s)$ (Hydrocerussite) + $4H^+$ ⇌ $3Pb^{2+} + 2HCO_3^- + 2H_2O$	2.41	(Edwards et al., 1992)
$PbSO_4(s)$ (Anglesite) ⇌ $Pb^{2+} + SO_4^{2-}$	-7.77	(Jang, 2023)
Aqueous Dissociation Reactions		
$PbCl^+$ ⇌ $Pb^{2+} + Cl^-$	-1.48	(Millero & Byrne, 1984)
$PbCl_2(aq)$ ⇌ $Pb^{2+} + 2Cl^-$	-2.03	(Millero & Byrne, 1984)
$PbCl_3^-$ ⇌ $Pb^{2+} + 3Cl^-$	-1.86	(Millero & Byrne, 1984)
$PbHCO_3^+$ ⇌ $Pb^{2+} + HCO_3^-$	-1.86	(Powell et al., 2009)
$PbCO_3(aq) + H^+$ ⇌ $Pb^{2+} + HCO_3^-$	3.88	(Powell et al., 2009)

Information Only

$Pb(CO_3)_2^{2-} + 2H^+ \rightleftharpoons Pb^{2+} + 2HCO_3^-$	10.53	(Powell et al., 2009)
$Pb(CO_3)OH^- + 2H^+ \rightleftharpoons Pb^{2+} + HCO_3^- + H_2O$	13.42	(Powell et al., 2009)
$Pb(CO_3)_3^{4-} + 3H^+ \rightleftharpoons Pb^{2+} + 3HCO_3^-$	27.19	(Jang, 2022)

Table GEOCHEM 4: Pitzer Interaction Parameters for the Lead system that are included in DATA0.FM6.

I	*j*	α_1/α_2	$\beta^{(0)}$	$\beta^{(1)}$	$\beta^{(2)}$	C^ϕ	Source
H^+	$PbCl_3^-$	2.0/12.0	0.1077	0.0425	0.00	-0.0035	(Jang, 2021)
Na^+	$PbCl_3^-$	2.0/12.0	-0.10025	0.0	0.0	0.0	(Jang et al., 2021b)
Mg^{2+}	$PbCl_3^-$	2.0/12.0	0.230125	0.0	0.0	0.0	(Domski, 2023c) after (Jang et al., 2021b)[3]
i	***j***	θ_{ij}					**Source**
H^+	Pb^{2+}	0.343					(Jang, 2023a)

GEOCHEM-3.10.2 The Iron System

The iron system, as presented by Kim et al. (Kim et al., 2017), was included in DATA0.FM6. Model parameters included were either derived by Kim et al. 2017 or originate in the literature. Table GEOCHEM 5 to Table GEOCHEM 8 include the parameters that are included in DATA0.FM6 for the iron system. Inclusion of the Iron - Sulfate system (Jang, 2023b) in DATA0.FM6 addresses EPA Issue 32 (Peake, 2022).

Table GEOCHEM 5: Equilibrium Constants for Reactions with Iron that are included in DATA0.FM6.

Reaction	log K	Source
Solid Dissolution Reactions		
$Fe(OH)_2(s) + 2H^+$ (ferrous hydroxide) $\rightleftharpoons Fe^{2+} + 2H_2O$	12.89	(Kim et al., 2017)
$Fe_2Cl(OH)_3(s) + 3H^+$ (hibbingite) $\rightleftharpoons 2Fe^{2+} + Cl^- + 3H_2O$	17.08	(Kim et al., 2017)
$FeCO_3(s) + H^+$ (siderite) $\rightleftharpoons Fe^{2+} + HCO_3^-$	-0.12	(Stumm & Morgan, 1996)

[3] The value of $\beta^{(0)}$ for Mg^{2+} - $PbCl^{3-}$ in Jang et al. (2021b) contains a transcription error, the correct value is documented in Domski (2023), and Table GEOCHEM 4 above.

Information Only

$Fe_2CO_3(OH)_2(s) + 3H^+$ (chukanovite) $\rightleftharpoons 2Fe^{2+} + HCO_3^- + 2H_2O$	12.32	(Kim et al., 2017)
$FeSO_4.H_2O(s)$ (Szomolnokite) $\rightleftharpoons Fe^{2+} + SO4^{2-} + H_2O$	-0.90	(Reardon & Beckie, 1987)
$FeSO_4.7H_2O(s)$ (Melanterite) $\rightleftharpoons Fe^{2+} + SO4^{2-} + 7H_2O$	-2.20	(Reardon & Beckie, 1987)
Aqueous Dissociation Reactions		
$FeOH^+ + H^+ \rightleftharpoons Fe^{2+} + H_2O$	9.31	(Shock et al., 1997)
$Fe(OH)_2(aq) + 2H^+ \rightleftharpoons Fe^{2+} + 2H_2O$	20.84	(Lemire et al., 2013) Jang et al. (2021b)
$Fe(OH)_3^- + 3H^+ \rightleftharpoons Fe^{2+} + 3H_2O$	31.0	(Baes & Mesmer, 1976)
$Fe(OH)_4^{2-} + 4H^+ \rightleftharpoons Fe^{2+} + 4H_2O$	46.00	(Baes & Mesmer, 1976)
$FeCO_3(aq) + H^+ \rightleftharpoons Fe^{2+} + HCO_3^-$	4.83	(Bruno et al., 1992)B
$Fe(CO_3)_2^{2-} + 2H^+ \rightleftharpoons Fe^{2+} + 2HCO_3^-$	13.89	(Kim et al., 2017)
$FeEDTA^{2-} \rightleftharpoons Fe^{2+} + EDTA^{4-}$	-16.1	(Morel & Hering, 1993)
$FeCitrate^- \rightleftharpoons Fe^{2+} + Citrate^{3-}$	-5.7	(Morel & Hering, 1993)
$FeOHCitrate^{2-} + H^+ \rightleftharpoons Fe^{2+} + Citrate^{3-} + H_2O$	2.24	(Jang et al., 2021b)

Table GEOCHEM 6: Pitzer Interaction Coefficients (Cation-Anion Interactions) for Ions Containing Iron that are included in DATA0.FM6.

i	*j*	α_1/α_2	$\beta^{(0)}$	$\beta^{(1)}$	$\beta^{(2)}$	C^ϕ	Source
Fe^{2+}	Cl^-	2.0/12.0	0.37324	1.13499	0.0	-0.02152	(Moog et al., 2004)
Na^+	$Fe(CO_3)_2^{2-}$	2.0/12.0	-0.230	6.26	0.0	0.0	(Kim et al., 2017)
Fe^{2+}	SO_4^{2-}	1.4/12.0	0.2568	3.063	-42.0	0.0209	(Reardon & Beckie, 1987)
Fe^{2+}	HSO_4^-	2.0/12.0	0.4273	3.48	0.0	0.0	(Reardon & Beckie, 1987)

Table GEOCHEM 7: Pitzer Interaction Coefficients (Cation-Cation Interactions) for Ions Containing Iron that are included in DATA0.FM6.

i	*j*	θ_{ij}	Source
Na^+	Fe^{2+}	0.10945	(Moog et al., 2004)
Mg^{2+}	Fe^{2+}	0.14504	(Moog et al., 2004)

Information Only

Table GEOCHEM 8: Pitzer Interaction Coefficients (Cation-Cation-Anion Interactions) for Ions Containing Iron that are included in DATA0.FM6.

i	*j*	*k*	ψ_{ijk}	Source
Fe^{2+}	Na^{+}	Cl^{-}	-0.01605	(Moog et al., 2004)
Fe^{2+}	Mg^{2+}	Cl^{-}	-0.02985	(Moog et al., 2004)
Fe^{2+}	HSO_4^{-}	Cl^{-}	0.0143	(Reardon & Beckie, 1987)

GEOCHEM-3.10.3 Magnesium Model

Jang (Jang, 2020) and Jang et al. (Jang et al., 2021) considered the MgOxalate·$2H_2O$(s) – Na_2Oxalate – H_2O system. The recommended log K values that were added to FM6 are summarized in Table GEOCHEM 9.

Table GEOCHEM 9: Reactions and log K values at 25 °C and I = 0 used for the Mg-Oxalate system.

Reaction	log K	Source
Solid Dissolution Reactions		
MgOxalate·$2H_2O$(s) (Glushinskite) ⇌ Mg^{2+} + $Oxalate^{2-}$ + 2H2O	-6.49	(Jang et al., 2021b)
Aqueous Dissociation Reactions		
$Mg(Oxalate)_2^{2-}$ ⇌ Mg^{2+} + 2$Oxalate^{2-}$	-4.94	(Martell, 1977)

GEOCHEM-3.10.4 Earlandite Solubility Product

The EPA noted in CC2-GEOCHEM-13 (Peake, 2020), and EPA Issue 29 (Peake, 2022) that the solubility product for earlandite ($Ca_3(Citrate)_2·4H_2O$) was omitted in DATA0.FM4 contrary to the analysis plan, AP-183, Rev.1 (Sisk-Scott, 2019a). The omission of the solubility product of earlandite by the DOE was an oversight that was corrected in DATA0.FM6. The solubility product for earlandite is presented in Table GEOCHEM 10.

Table GEOCHEM 10: Solubility constant of Earlandite ($Ca_3(Citrate)_2·4H_2O$) to be implemented in DATA0.FM6.

Reaction	log K	Source
Solid Dissolution Reactions		
$Ca_3(Citrate)_2·4H_2O$ ⇌ 3Ca^{2+} + 2$Citrate^{3-}$ + $4H_2O$	-17.9	(Hummel et al., 2005)

Information Only

GEOCHEM-4.0 Dissolved Actinide Source Term Process Model

The WIPP thermodynamic database (Domski & Nemer, 2023a) was updated for the RPPCR from DATA0.FM1 database to DATA0.FM6 to include a new Am – Hydroxide solid polymorph solubility constant, and a Pitzer parameter for the $Am(OH)_2^+$ / Mg^{2+} pair as documented in Jang et al. (Jang, 2021). This update to the An(III) solubility model addressed Issue 10 outlined in (Peake, 2022) which was concerned with the crystallinity of the An(III) solubility controlling phase. Neither the An(IV) or An(V) thermodynamic models were updated for RPPCR, and the reader is directed to the CRA-2019 DPA Appendix GEOCHEM Section 4.3 for a discussion of these models.

For a detailed discussion of the legacy parameters included in DATA0.FM1, and thus, DATA0.FM6, the reader is directed to the CRA-2019 DPA Appendix GEOCHEM Section 4.2.

GEOCHEM-4.1 The An(III) Model

Jang et al. (Jang, 2021) tested if the current An(III) model used in DATA0.FM1 would accurately predict the solubility of $Nd(OH)_3(s)$ as a function of incremental $MgCl_2$ ($Nd(OH)_3(s)$ - $MgCl_2$ - H_2O system). Model parametrization was performed using the solubility constant log K(Nd(OH)3(s)) = 16.9 (Guillaumont et al., 2003) along with an updated Pitzer interaction parameter (PIP) $\theta(Nd(OH)_2^+/Mg^{2+}) = 0.302$.

Table GEOCHEM 11: Recommendation of new Pitzer parameters for the $Nd(OH)_3(s)$ - $MgCl_2$ - H_2O system. Note: Nd(III) is an analog for Am(III).

Reaction		log K	Source
Solid Dissolution Reactions			
$Am(OH)_3(am) + 3H^+ \rightleftharpoons Am^{3+} + 3H_2O$		16.9	(Guillaumont et al., 2003)
i	***j***	θij	**Source**
$Am(OH)_2^+$	Mg^{2+}	0.302	(Jang, 2021)

GEOCHEM-4.2 Comparison of An(III) Models

For CRA-2014 and 2019 DPA the EPA had three concerns regarding the An(III) model used to calculate +III actinide solubilities: 1) Issue 23 (Peake, 2018) the EPA requested examination of the (Neck et al., 2009) An(III) model; 2) issue 10 (Peake, 2022) addressed the crystallinity of the An(III) solubility controlling phase used in the actinide uncertainty analysis; and 3) issue 11 (Peake, 2022) questions the An(III) Pitzer parameters in the WIPP model documented in (Oakes et al., 2021). These three issues are discussed in the following sections and were presented at the October 2022 Technical Exchange between the EPA and DOE (Miller et al., 2022).

Information Only

GEOCHEM-4.3 The Neck et al. (2009) An(III) Model

To address EPA Issue 23 (Peake, 2018) SNL did an analysis of the (Neck et al., 2009) study (Domski, 2022), hereafter the "Neck model". Only a broad summary of Domski will be provided herein. Neck et al. performed undersaturation experiments using $Nd(OH)_3(cr)$, which was used as the solubility controlling phase in matrix solutions of NaCl, $MgCl_2$, and $CaCl_2$ of 0.1, 0.5, 2.5, and 5.0 M for NaCl, and 0.25, 1.0, 2.5, 3.5 M for $MgCl_2$, and $CaCl_2$. The Neck et al. laboratory solubility data which is most representative of expected WIPP conditions are those collected in 5.0 M NaCl, 0.25 $MgCl_2$, and $CaCl_2$ matrix solutions. These are compared to the WIPP An(III) model below.

Based on their experimental data, (Neck et al., 2009) derived a log K value for the $Nd(OH)_3(s)$ phase, and Neck states that their derived value falls between that recommended by (Baes & Mesmer, 1976) of 18.66 ± 0.55 *for fresh, amorphous precipitates of Nd(OH)3(s) and 16.02 ± 0.37 for aged and crystalline Nd(OH)3(s).* Since a crystalline form of $Nd(OH)_3$ was identified in the post-test solids analysis of (Neck et al., 2009) it may be expected that the derived log K would reflect the higher crystallinity, however, the issue of Am-hydroxide crystallinity as it relates to solubility is not straightforward.

From (Neck et al., 2009):

> *The use of the notation "crystalline" and "amorphous" to describe a solid phase and thereby its solubility is an oversimplification. The X-ray diffraction (XRD) data give only information of the bulk structure, while the solubility is determined by the surface characteristics or by fractions of smaller ("amorphous") particles included in a bulk crystalline solid.*

This observation may explain why Neck's value of log K for $Nd(OH)_3(s)$ (17.2 ± 0.4) is intermediate between the amorphous and crystalline values of other authors. That is, while the system is far from equilibrium, the XRD only detects the crystalline phase, whereas the solubility experimental measurements reflect the most soluble fraction of the $Nd(OH)_3$ solid.

Figure GEOCHEM 1 below, recreates Figures 1D and 2A from (Domski, 2022) showing the Neck model (both log K values and Pitzer parameters) fit to the experimental data of (Neck et al., 2009). Figure GEOCHEM 1 shows that the Neck derived log K value fits their measured NaCl, $MgCl_2$, and $CaCl_2$ data very well, as would be expected.

Information Only

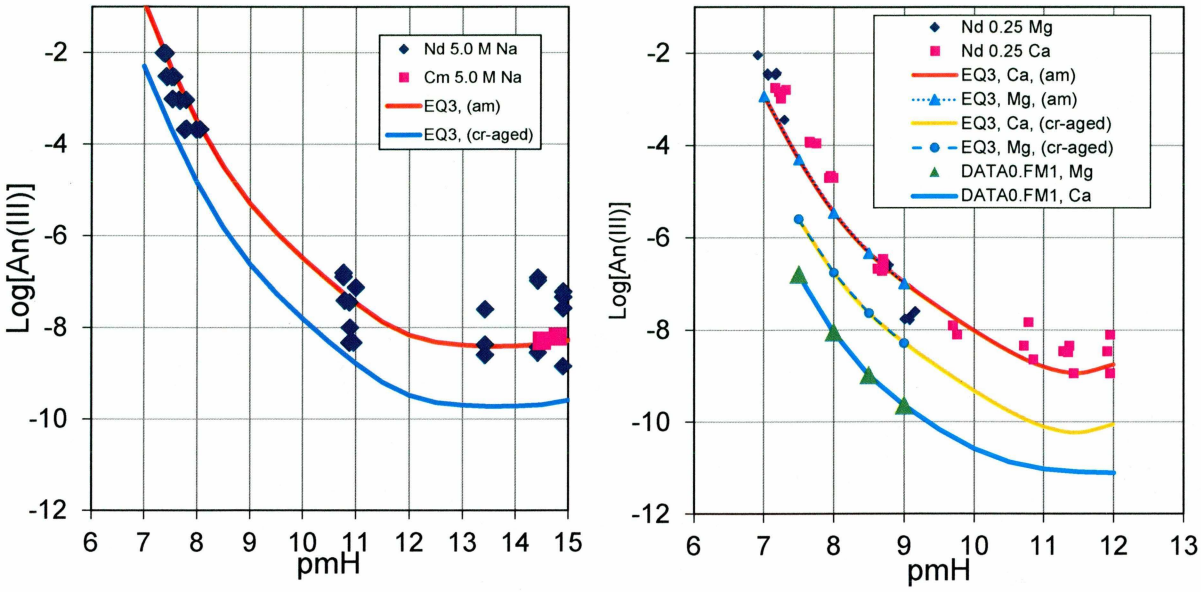

Figure GEOCHEM 1: From (Domski, 2022) Figure 1D and Figure 2A, for 5.0 M NaCl and 0.25 M $MgCl_2$ and $MgCl_2$ solutions, showing the measured data as symbols and EQ3/6 simulated data as lines.

In addition to implementing the Neck model in the EQ3/6 database, (Domski, 2022) also examined the stability field of Am(III) solids for WIPP conditions and applied the Neck model to the CRA-2019 DPA actinide solubility model. The results showed that for WIPP conditions $AmOHCO_3$(c) was more stable than $Am(OH)_3$(am), and that $Am(OH)_3$(s) was more stable than $AmOHCO_3$(c). Thus, if the least soluble form of Am – Hydroxide [$Am(OH)_3$(s)] is suppressed (Domski, 2022), then $AmOHCO_3$(c) becomes the solubility controlling phase in the WIPP.

Application of the Neck model to the CRA-2019 DPA baseline solubility model was done for both brine types, GWB and ERDA-6, at the minimum brine, 1X, brine volume. The results confirmed that with the least soluble form of Am – Hydroxide suppressed $AmOHCO_3$(c) became the solubility controlling phase for both brine types. In addition, the total An(III) concentration was virtually unchanged, in other words, there was no impact on the An(III) concentration.

GEOCHEM-4.4 The Oakes et al. (2021) An(III) Model

In Issue 11 (Peake, 2022), the EPA expressed that they wanted the DOE to investigate potential errors identified by (Oakes et al., 2021). From page B-45 of the EPA TECHNICAL SUPPORT DOCUMENT FOR SECTION 194.24 (EPA, 2022):

(Oakes et al., 2021). evaluated the available +III actinide data, and had difficulty reproducing some of the figures from Könnecke et al. (1997). (Oakes et al., 2021) concluded that there are potential internal inconsistencies in the WIPP Am(III) model that was derived from (Könnecke et

Information Only

al., 1997), which could affect the log β^0 values for $AmCl^{2+}$ and $AmCl_2^+$ and some of the Pitzer parameters. DOE should evaluate these possible inconsistencies prior to the next WIPP PA.

(Oakes et al., 2021), pages 315-316 stated that, *...the WIPP thermodynamic model cited by (Xiong et al., 2017) is internally inconsistent.* Oakes claim appears to be based on their inability to reproduce Fig. 3 of (Könnecke et al., 1997) using the parameters listed.

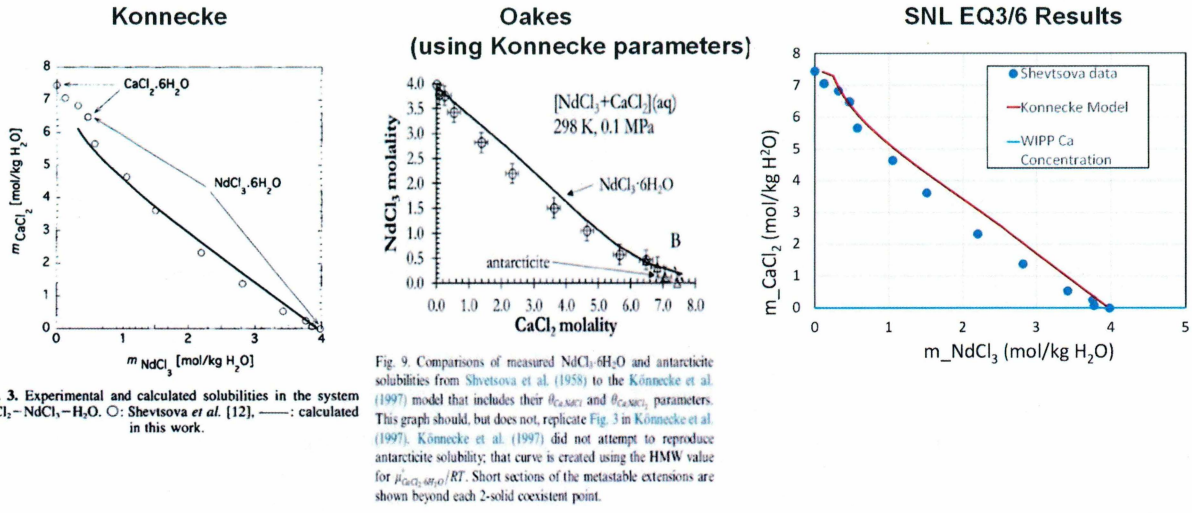

Fig. 3. Experimental and calculated solubilities in the system $CaCl_2-NdCl_3-H_2O$. ○: Shevtsova *et al.* [12], ——: calculated in this work.

Fig. 9. Comparisons of measured $NdCl_3 \cdot 6H_2O$ and antarcticite solubilities from Shvetsova et al. (1958) to the Könnecke et al. (1997) model that includes their $\theta_{Ca,NdCl}$ and $\theta_{Ca,NdCl_2}$ parameters. This graph should, but does not, replicate Fig. 3 in Könnecke et al. (1997). Könnecke et al. (1997) did not attempt to reproduce antarcticite solubility; that curve is created using the HMW value for $\mu^{\circ}_{CaCl_2 \cdot 6H_2O}/RT$. Short sections of the metastable extensions are shown beyond each 2-solid coexistent point.

Figure GEOCHEM 2: Comparison of Konnecke et al. (1997), Oakes et al. (2021) and EQ3/6 results of SNL. Note that on the figure of Oakes et al. (2021) the axes are reversed from that of the original work by Konnecke.

As shown in Figure GEOCHEM 2, the difference in the simulated data of the three different sources is relatively small. Given the relatively small differences, and that neither the codes nor the manner in which the simulations were performed was specified in (Könnecke et al., 1997) and (Oakes et al., 2021), we conclude that the cause(s) of differences shown in Figure GEOCHEM 2 remain uncertain. Furthermore, the concentration of Ca^{2+} of WIPP brines is about 0.02 molal, which is close to zero on the scale of Figure GEOCHEM 2, meaning that the influence of Calcium - Chloride aqueous species is negligible for the purposes of WIPP actinide solubility calculations.

To determine the effect that the Am - Cl system had on the CRA-2019 DPA baseline actinide solubility model a database was constructed from the WIPP database, DATA0.FM5, that implemented the full (Oakes et al., 2021) model as presented in Tables 3, 4, and 5 of (Oakes et al., 2021); This database was called DATA0.OK5. The minimum volume case, 1x volume, was run for the GWB brine type, using the same solubility controlling phases, and the species concentrations were extracted from the output files. Table GEOCHEM 12 provides the Am - Cl aqueous species concentration for the CRA-2019 DPA. These results show that the Am - Cl species concentrations are ~5 to 9 orders of magnitude less than the expected total Am(III) dissolved concentration of ~2E-07 molal. At these low concentrations, the Am - Cl species are

Information Only

inconsequential, in other words, their contribution to the total dissolved Am(III) concentration is negligible at the expected WIPP repository conditions, this is true for both the WIPP and Oakes models.

Table GEOCHEM 12: Am – Cl aqueous species concentrations.

	GWB			
Model	**WIPP**	**Oakes**	**WIPP**	**Oakes**
Species/DB	DATA0.FM5	DATA0.OK5	DATA0.FM5	DATA0.OK5
$AmCl^{2+}$ Molality	9.84E-13	2.49E-16	7.68E-13	1.93E-16
$AmCl_2^{+}$ Molality	3.93E-14	4.58E-16	2.99E-14	4.10E-16

If there are issues with the (Könnecke et al., 1997) Am - Cl model as implemented in the *WIPP thermodynamic model*, then it had no effect on the CRA-2019 total dissolved Am(III) concentration and is not expected to impact actinide solubilities for future silubility calculations. This work was presented at the October Technical Exchange between the EPA and DOE and is documented in (Miller et al., 2022).

GEOCHEM-4.5 Comparison the WIPP, Neck, and Oakes Models for An(III) Solubility

To compare the WIPP An(III) model to that of Neck and Oakes, simulations comparing the three models to An(III) solubility data measured in 5 M NaCl from various authors were plotted (Figure GEOCHEM 3). The first feature of note in Figure GEOCHEM 3 is the scatter in the measured An(III) concentrations, which in extreme cases is 3 log units at a fixed pH value. This spread in concentration highlights the difficulty and uncertainty of measuring concentrations at such low levels. The second feature to notice in Figure GEOCHEM 3 is that all of the models provide an adequate fit when the spread in the measured data is considered. For the purposes of WIPP the most conservative model, Model 1, has been employed for the RPPCR (Domski, 2023c). This amounts to a net bias towards greater solubility than would be inferred from the majority of the data alone.

Information Only

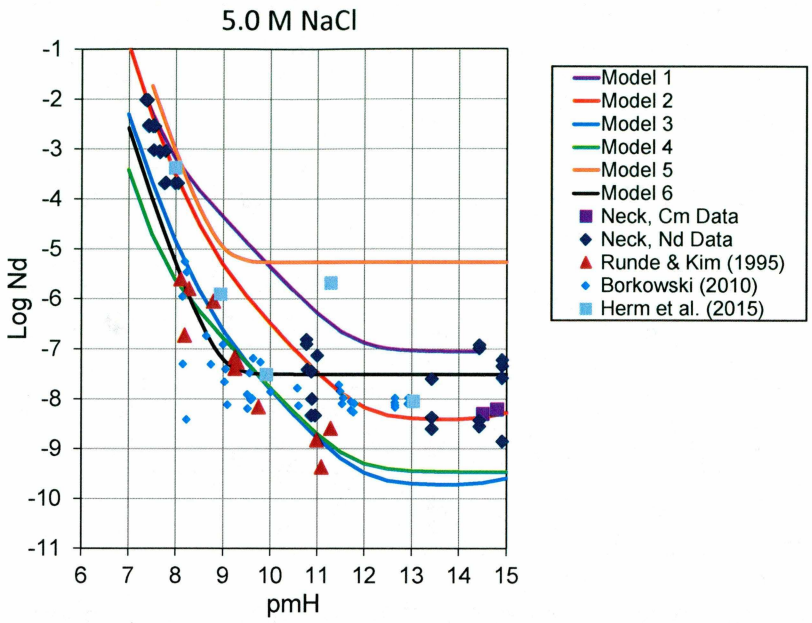

Figure GEOCHEM 3: An(III) models compared to measured An(III) data (see below for model descriptions.

1. Model 1: DATA0.FM1 with the Am(OH)3(am) log K (16.9) of (Guillaumont et al., 2003) from (Jang et al., 2021) used in DATA0.FM6;
2. Model 2 and 3: DATA0.FM1 with the (Neck et al., 2009) model fully implemented (i.e., Log K values of aqueous species and Pitzer parameters), Model 2 using the $Am(OH)_3$(am) log K, and
3. Model 3 $Am(OH)_3$(cr-aged) values of (Guillaumont et al., 2003) as recommended by Neck, and documented in (Domski, 2022);
4. Model 4: DATA0.FM1 $Am(OH)_3$(s) Solubility controlling phase;
5. Model 5 and 6: (Oakes et al., 2021) fully implemented as a singular set of parameters with no other parameters included. Model 5 uses Oakes amorphous phase $Am(OH)_3$(am) and Model 6 uses the crystalline phase $Am(OH)_3$(cr).

The EPA concerns with the An(III) model, Issue 23 (Peake, 2018), Issue 10 and 11 (Peake, 2022), were addressed and applied to the RPPCR (Domski, 2023c), and summarized in the above sections. As has been demonstrated, the current model provides a conservative assessment of total An(III) solubility.

Information Only

GEOCHEM-5.0 Dissolved Actinide Source Term Quantification of Uncertainty Summary

In terms of the chemical conditions and actinide source term process models, the only uncertainties that are quantified for the purposes of performance assessment are uncertainties in the parametrization of the An(III) and An(IV) models of the dissolved actinide source term process model. Other uncertainties include conceptual model and process model uncertainty, neither of which is quantified for performance assessment purposes. Section 4.4 of the CRA-2019 DPA Appendix Geochem provides an in-depth examination of uncertainties associated with conceptual model, process model, and process model parameterization. These discussions will not be repeated except when a change or an update to the CRA-2019 models have been implemented.

The RPPCR actinide uncertainty analysis differs from that documented in (R. Knerr, 2021), which addresses the EPA comment CC1-GEOCHEM-1 for the CRA-2019 DPA by the following: 1) A new literature search was performed; 2) new literature screening criteria (Domski & Nemer, 2023b) were applied to the experimental studies used to compare the WIPP models; and 3) an updated WIPP database, DATA0.FM6 (Domski, 2023c) was used.

GEOCHEM-5.1 Literature Screening Criteria for Actinide Uncertainty Analysis

An update to the literature screening criteria was facilitated by DOE, SNL, and Los Alamos National Laboratory, and is documented in (Domski & Nemer, 2023b). The motivation to revise the existing screening criteria was to simplify the language for clarity and refine the experimental data selection strategies. The primary objective is to test the solubility models under the chemical conditions for which it is used in PA, i.e., the expected post-closure repository conditions. Issue 9 (Peake, 2022) specifies that the literature cutoff date for the uncertainty analysis be defined and the updated criterion 1 addresses this issue. The update to the screening criteria is documented in (Domski & Nemer, 2023b).

The WIPP literature screening criteria are used to determine which experimental studies, or specific data, or subsets of data, from an experimental study, are included in the actinide uncertainty analysis. Each of the screening criteria must be met for a study to be included in the uncertainty analysis. However, exceptions may be considered on a case-by-case basis, provided any exception is technically justified and is well documented. These screening criteria are intended for use in the WIPP actinide uncertainty analysis, they are NOT intended to be used to select parameters to be included in the WIPP actinide solubility model, i.e., the thermodynamic database. The purpose of the criteria is to test the WIPP thermodynamic models of the +III and +IV actinides for conditions which mostly closely resemble those expected in the WIPP post-closure environment.

Information Only

GEOCHEM-5.2 Literature Screening

A new literature search was initiated for the RPPCR. This literature search was broader than previous searches in accordance with criteria G1 and G6 (Domski & Nemer, 2023b). The literature search cutoff date for the RPPCR was October 9, 2022, which is 3-months before the data cutoff date. The starting date for the literature search was not specified as criterion G1 does not specify a start date. This broad-based screening was facilitated using Python scripts to search two databases: 1) Web of Science, to obtain journal articles and conference papers (https://app.webofknowledge.com/author/search), and 2) OSTI, to obtain US government reports (i.e., the G2 criterion) (https://www.osti.gov). The Python scripts and their application are explained in (Domski & Nemer, 2023b). The updated literature screening criteria G1 (Domski, 2023b) directly address and resolve Issue 9 of the EPA (Peake, 2022) by setting and implementing a cutoff date for the eligible literature inclusion date.

The literature screening completed for the RPPCR identified 8 potential experimental studies for the An(IV) actinides. However, a detailed examination of these studies revealed that zero met all of the screening criteria (see below), and as such zero new literature data were included in the current An(IV) uncertainty analysis. Re-screening of previously screened literature using the new criteria (Domski & Nemer, 2023b) identified an additional two data points from the (Altmaier et al., 2004) reference. These two data points were included with the five data points that resulted from the application of the new G10 criterion as reported by (Domski & Nemer, 2023b) for the An(IV) uncertainty distribution.

The An(III) literature screening identified one potential solubility study which required in-depth screening to determine eligibility for the RPPCR uncertainty analysis, however, this study did not meet all of the screening criteria, and thus, provided no new data. Literature previously screened for past uncertainty analyses was re-screened for the RPPCR and did not identify any additional data that could be used in the RPPCR An(III) uncertainty analysis. However, re-screening of the An(III) references provided in (M. Knerr, 2021) eliminated 97 of the 129 data previous screened in the uncertainty analysis. Therefore, the RPPCR An(III) uncertainty analysis includes 30 experimental data points.

GEOCHEM-5.3 An(IV) Actinide Uncertainty Analysis

The results of the An(IV) actinide uncertainty analysis may be found in the following analysis reports for this task: for the RPPCR,(Domski, 2023b).

The histogram and empirical cumulative distribution function (CDF) plots for the +IV actinides are provided for the RPPCR (Domski, 2023b) in Figure GEOCHEM 4 and Figure GEOCHEM 5, respectively.

Information Only

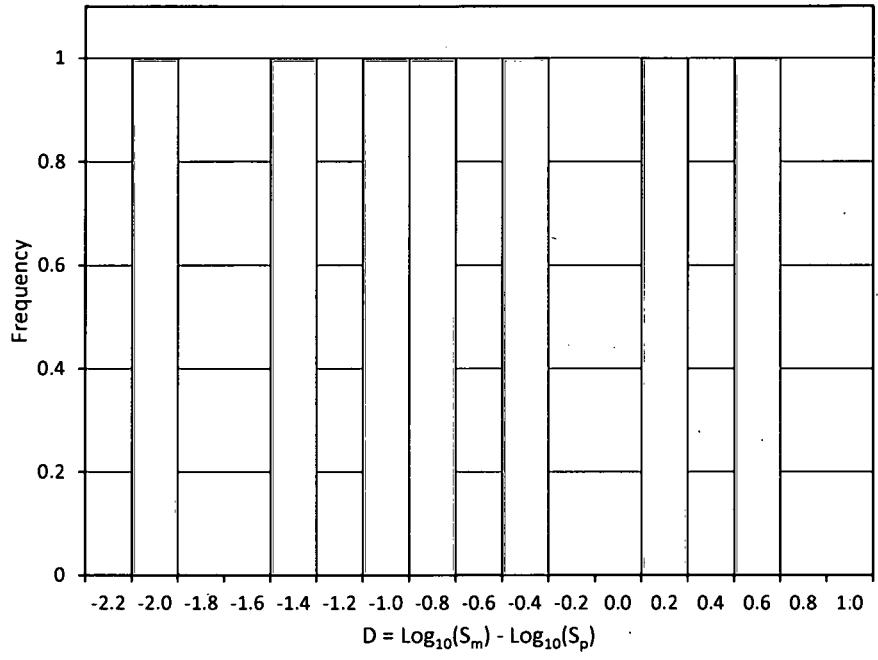

Figure GEOCHEM 4: Histogram for the RPPCR of the difference D = log10 Sm – log10 Sp for Th(IV).

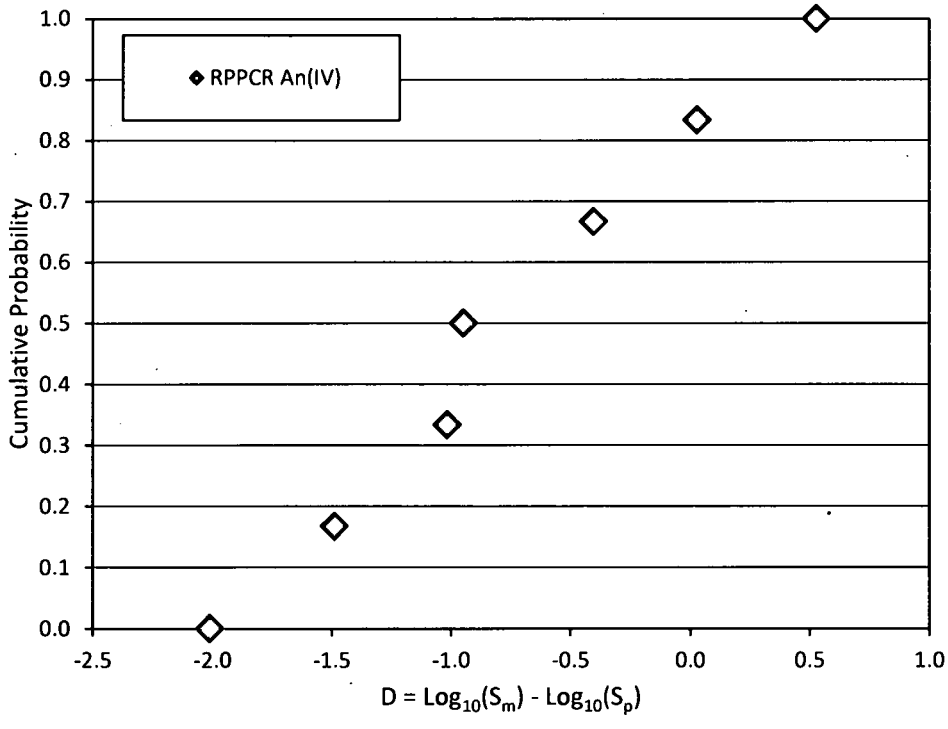

Figure GEOCHEM 5: CDF plot for the RPPCR of the difference D = log10 Sm – log10 Sp for Th(IV).

Information Only

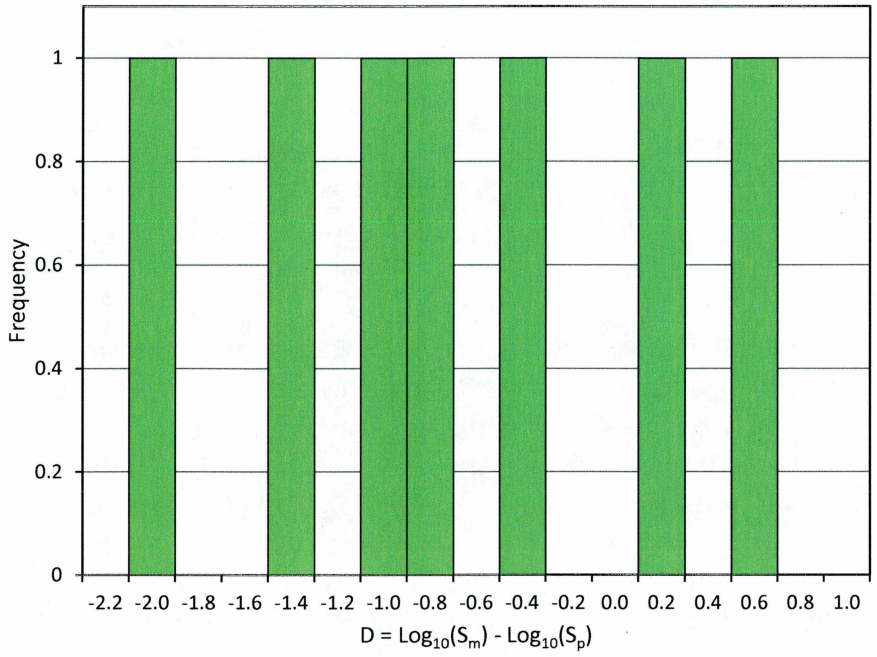

Figure GEOCHEM 4: Histogram for the RPPCR of the difference D = log10 Sm – log10 Sp for Th(IV).

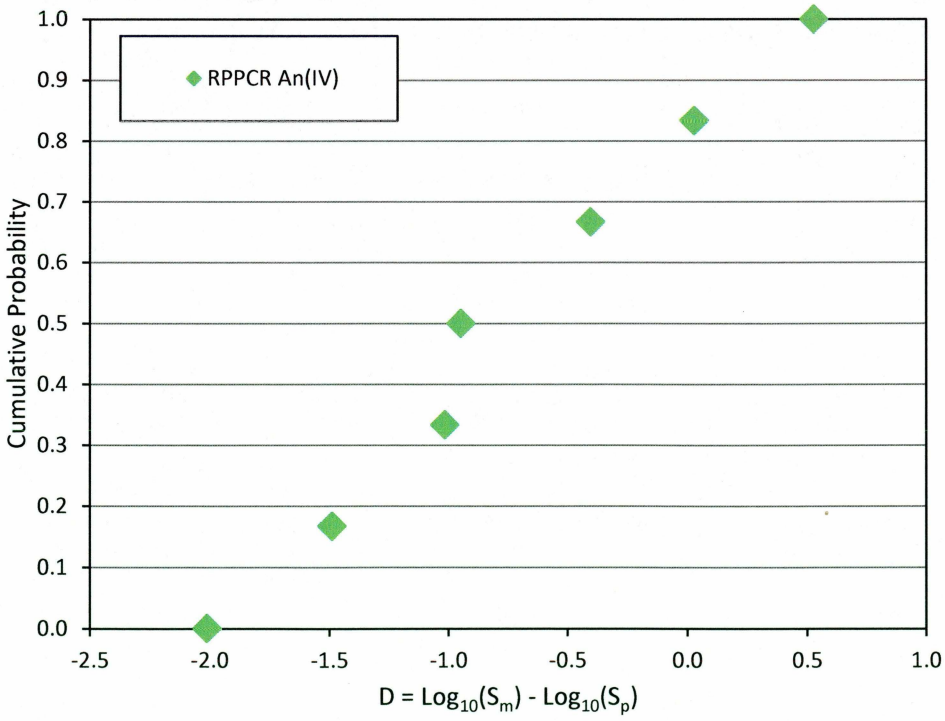

Figure GEOCHEM 5: CDF plot for the RPPCR of the difference D = log10 Sm – log10 Sp for Th(IV).

Information Only

Table GEOCHEM 13: Statistical Properties of the Distribution of D = log10(Sm) – log10(Sp) for Th(IV) for the RPPCR compared with the CRA-2019 DPA data (Domski, 2019b).

Analysis	Mean	Median	Standard Deviation	Minimum	Maximum
CRA-2019 DPA	–0.0114	–0.0900	0.821	–2.01	1.43
RPPCR	-0.758	-0.947	0.876	-2.01	0.53

The results of the RPPCR uncertainty analysis show that the mean and maximum of the distribution is shifted to smaller (more negative in terms of the mean) values compared to the CRA-2019 DPA. The cause of the shift was the application of the update G10 criterion which eliminated data that was underpredicting the Th(IV) solubility. The Th(IV) model included in DATA0.FM6 is the same as that in the database used, DATA0.FM4 (Domski, 2019a), therefore, there was no impact of using the new database on the calculated Th(IV) concentrations.

GEOCHEM-5.4 An(III) Actinide Uncertainty Analysis

The results of the An(III) actinide uncertainty analysis may be found in the analysis report for this task, for the RPPCR,(Domski, 2023b).

The histogram and empirical CDF plots for the +III actinides are provided for the RPPCR (Domski, 2023b) in Figure GEOCHEM 6 and Figure GEOCHEM 7, respectively.

Information Only

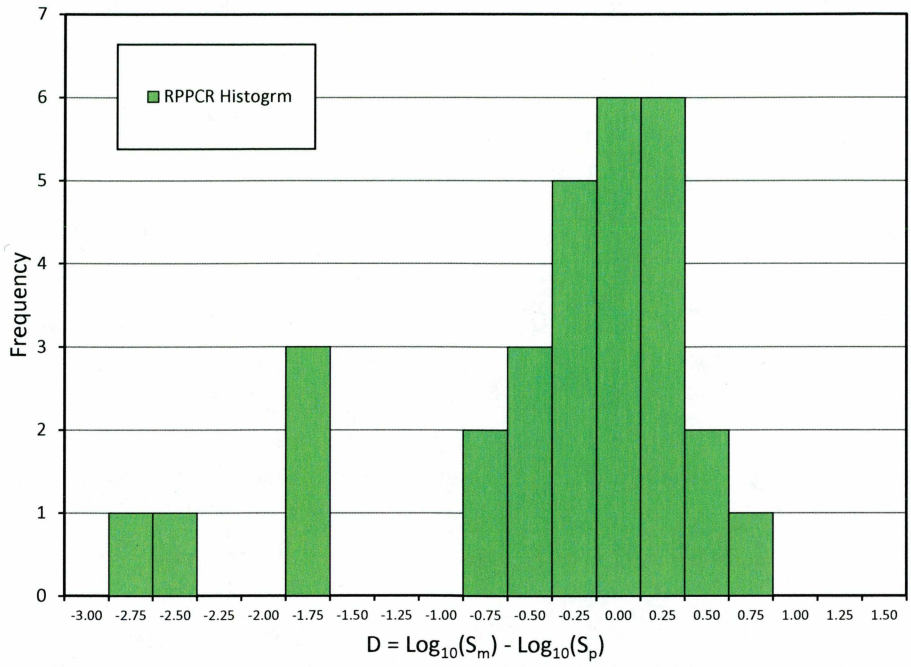

Figure GEOCHEM 6: Histogram for the RPPCR of the difference D = log10 Sm – log10 Sp Am(III).

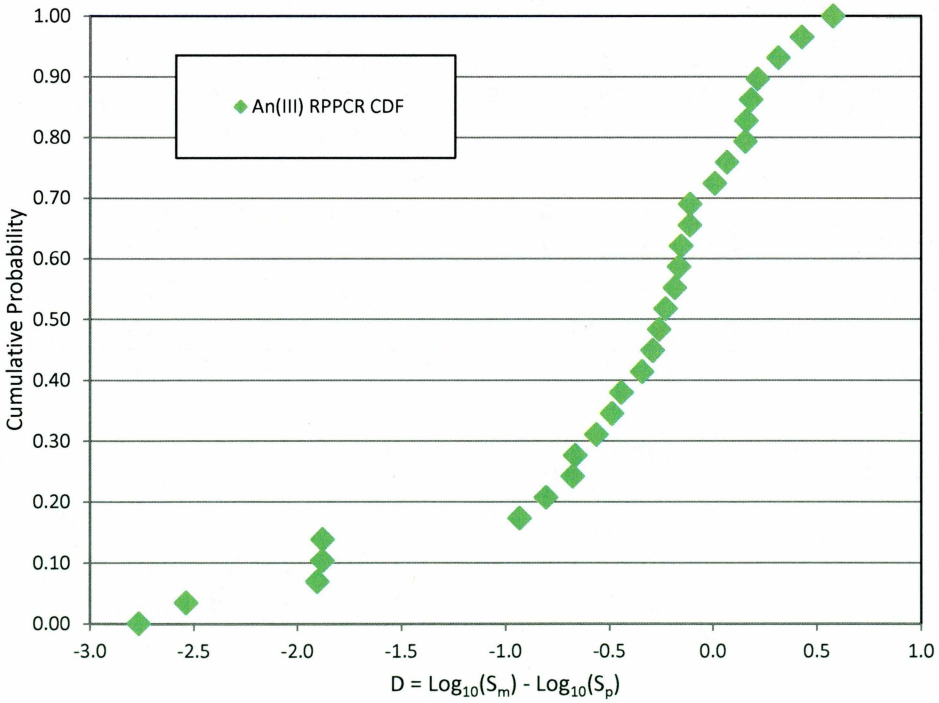

Figure GEOCHEM 7: CDF plot for the RPPCR of the difference D = log10 Sm – log10 Sp for Am(III).

Information Only

Table GEOCHEM 14: Statistical Properties of the Distribution of D = log10(Sm) – log10(Sp) for An(III) for RPPCR compared with the CRA-2019 DPA data (Domski, 2019b).

Analysis	Mean	Median	Standard Deviation	Minimum	Maximum
CRA-2019 DPA	0.651	0.516	1.01	-1.14	2.97
RPPCR	-0.509	-0.245	0.858	-2.76	0.578

Compared to the CRA-2019 DPA results the RPPCR results are shifted toward negative values. This is direct result of two factors: 1) The use of the amorphous form of Am-hydroxide as the solubility-controlling phase which tends to provide a better fit to the measured data, albeit the fits may tend to slightly overestimate the An(III) solubility resulting in small negative values; and 2) the updated literature screening criteria which eliminated some studies from consideration.

GEOCHEM-5.5 Conclusions of the Actinide Uncertainty Analysis

The RPPCR actinide uncertainty analysis were presented in (Domski, 2023b) respectively. These actinide uncertainty analyses differ from past analysis by the use of an updated WIPP database which incorporates an additional Am-hydroxide polymorph of higher solubility (Jang et al., 2021) than that used in previous actinide uncertainty analyses (e.g., (Brush & Domski, 2013; Domski, 2019b; R. Knerr, 2021). Additionally, the current analysis implemented the updated literature screening criteria of (Domski & Nemer, 2023b), which has three significant changes compared to the criteria used in previous analyses:

1) G1: Allows pre-1990 publications and sets the cutoff date to three months prior to the required parameter feed to performance assessment for the current recertification cycle, which was 10/09/2022 for the current analysis.
2) G6: Allows for consideration of solubility studies from additional oxidation-state analogs for the An(III) and An(IV) uncertainty analyses. The An(III) model considered Am(III), Nd(III), Cm(III), and Pu(III). The An(IV) model considered Th(IV), Pu(IV) and U(IV) studies.
3) G10: The WIPP conditions criterion was refined to be more specific to expected WIPP conditions.

With the specification of the end date for the literature search in criterion G1, EPA Issue 9 has been resolved. Likewise, the addition of the amorphous form of Am-hydroxide to DATA0.FM6 (Domski, 2023c), and the use of this phase, with two other Am(III) phases, in the RPPCR An(III) actinide uncertainty analysis addresses the concerns of EPA Issue 10 (Peake, 2022) by using more appropriate phases to simulate experimental data where less-crystalline, more soluble solid phases may have been controlling solubility.

Information Only

GEOCHEM-6.0 Gas Generation and Metal Corrosion

Iron (Fe) is the primary constituent of the metal alloys that are used to contain contact-handled and remote-handled waste in the WIPP (Van Soest, 2022). When all the waste is emplaced, it is estimated that the WIPP will contain over 74,500 metric tons of Fe (Van Soest, 2022). Corrosion will occur once the repository is sealed and the emplaced Fe comes into contact with brine either through seepage or an intrusion event (DOE, 2019c). Corrosion is considered the main contributor of gas generation in the repository (DOE, 2019a). It is expected that corrosion will reduce the oxidation state of some of the actinides and affect their solubility, binding constants, and therefore mobility (Altmaier et al., 2009; DOE, 2019d; Felmy et al., 2011; Rai et al., 2002; Reed et al., 2006). Corrosion rate, products, and gas generation are all variables that can help predict actinide availability.

Corrosion is an electrochemical process, where a metal loses an electron, becoming oxidized in the process. Since electrons do not exist freely in solution, reduction/oxidation (redox) reactions are always coupled. In the repository, it is assumed that the oxidation of Fe will be coupled to the reduction of water and the associated production of gaseous hydrogen (H_2). The anoxic Fe corrosion reactions in the WIPP gas generation process model that will produce H_2 are assumed to be the oxidation of Fe to ferrous hydroxide ($Fe(OH)_2$) (Eq 4) and magnetite (Fe_3O_4) (Eq 5). Thermodynamically, $Fe(OH)_2$ is less stable than Fe_3O_4 and on longer time scales $Fe(OH)_2$ may convert to Fe_3O_4 (2) (Schikorr, 1933).

$$Fe(s) + 2\,H_2O \rightarrow Fe(OH)_2(s) + H_2(g) \qquad (Eq\ 4)$$

$$3\,Fe(s) + 4\,H_2O(l) \rightarrow Fe_3O_4(s) + 4\,H_2(g) \qquad (Eq\ 5)$$

Note: Eq 4 and 5 delineate reactions for the thermodynamically predicted corrosion products. For experimentally derived corrosion products see section 2.2.

GEOCHEM-6.1 Parameterization Uncertainties

As of the CRA-2019 there is still uncertainty in the parameterization of the process models with respect to Fe corrosion. Uncertainties as they pertain to Fe corrosion include corrosion rates, corrosion products, gas generation, and others.

Note: Passivation reactions screened out in CRA-2019 are no longer included here (CO_2 and H_2S) based on the results of the SEN4 study (EPA, 2017). DOE agreed to remove reactions from the model related to steel corrosion by sulfide to represent passivation for CRA-2019.

GEOCHEM-6.1.1 Corrosion Rates

Reaction rates of metallic Fe conversion to $Fe(OH)_2$, and Fe_3O_4 remain uncertain. There is variability between datasets and methods used to measure corrosion rates. Method variability may be due to different approaches providing different types of data. For example, mass loss measures the average corrosion rate while electrochemical methods measure instantaneous rates, so direct method comparisons should not be made. The differences between datasets for

Information Only

similar methods are most likely due to effects of the different types of materials and their elemental composition. There are over twenty different types of steel used to contain waste in the repository. Most of these steels have varying grades which also contribute to differences in their composition. There are thirteen different elements that make up the steels used in the repository. Corrosion rates are affected by the variances in those elements (Clover et al., 2005; Guo et al., 2009). Figure GEOCHEM 8 outlines the variations in elemental composition for the steels used in the WIPP (Pavitt, 2024; WIPP, 2023). The corrosion rates currently used in the PA calculations are based on the results from 2013 (Roselle, 2013).

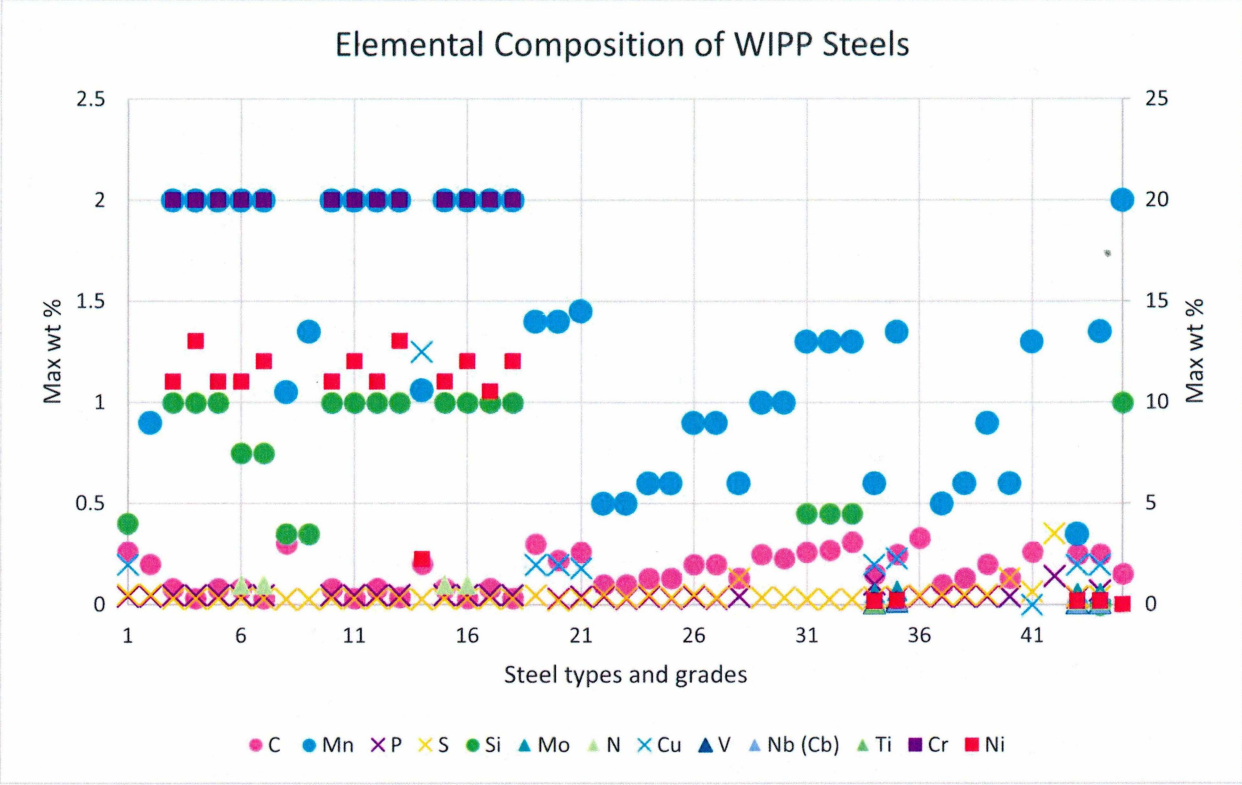

Figure GEOCHEM 8: Variance in the elemental composition of the different types of steel and grades used in the WIPP. Different elements are denoted by different colors. Square markers correspond to the right y-axis, all other markers use the left y-axis. X-markers represent elements whose composition does not vary greatly; triangle markers represent elements that are in less than 10% of the steel listed.

GEOCHEM-6.1.2 Corrosion Products

WIPP-specific experiments have produced mixed results in terms of corrosion products. Early XRD experiments at various overpressures showed reevesite for H_2 overpressure (Telander & Westerman, 1993; Telander & Westerman, 1997), but this was inconclusive as there was a possible contamination by the Ni-Cr-Mo alloy autoclave. A greenish-grey corrosion product was noted but "could not be identified with XRD" (Telander & Westerman, 1993). Long term mass loss tests produced equivalent moles of H_2 for every Fe reacted (assuming divalent Fe only),

Information Only

consistent with Eq 4. Roselle's scanning electron microscopy (SEM) results indicated an iron-chloro-hydroxide (with little or no Mg) and a visible green corrosion product was noted (Roselle, 2009, 2010, 2011a, 2011b). Nemer et al. suspected hibbingite ($Fe_2(OH)_3Cl$) as a significant corrosion product although this was only assumed and could not be fully verified using XRD (Nemer et al., 2011). Sisk-Scott observed Fe_3O_4 at elevated temperature (Sisk-Scott, 2019b). Fe_3O_4 has been observed to form as a corrosion product at elevated temperatures and under oxic conditions (Haberman & Frydrych, 1988); a literature review and research are being conducted to conclude whether it will form at WIPP repository temperatures (27°C) under anoxic conditions (Odziemkowski et al., 1998). Currently, only the iron hydroxide (Eq 4) reaction is implemented in the PA calculations. The current EPA position is to continue to evaluate available data to determine if gas production stoichiometry should be re-evaluated (Peake, 2022).

GEOCHEM-6.1.3 Gas Generation

The H_2 gas production rate remains uncertain. In addition, there is uncertainty in the literature as to the impact of increased pressure on corrosion rates. Higher nitrogen (N_2) pressures, between 1-7 MPa have been observed to increase corrosion rates, although above 7 (up to 13) MPa no further increase was observed (Telander & Westerman, 1997). Under H_2 pressure, corrosion rates have been observed to reach a maximum at 0.2 MPa and a minimum at pressure of 4 to 7 MPa (Telander & Westerman, 1993; Telander & Westerman, 1997). Sun and Liu (Liu et al., 2021; Sun et al., 2013) observed an increased corrosion rate in N_2, but a decrease in H_2, consistent with Telander and Westerman. Smart et al. noted no effect on corrosion rate or electrochemical potential at H_2 overpressures up to 10 MPa (Smart et al., 2001).

GEOCHEM-6.1.4 Other Uncertainties

- Extent of surface passivation on steel alloys.
- Potential for oxic corrosion to continue (all oxygen will be consumed within 100 years) due to radiolysis of brine.
- Will aluminum (Al), which is approximately 1% by mass of the amount of steel emplaced in the WIPP (Van Soest, 2022) increase corrosion rates due to galvanic coupling between Fe and Al. In addition, there have been reports of galvanic coupling between metals and non-metals (Qiu et al., 2020). Currently galvanic coupling between different types of steel, different types of metals, and between metals and non-metals has been screened out in the Feature, Event, and Processes Screening for PA (DOE, 2019c). The current EPA position is to continue to screen out galvanic corrosion, but the screening argument should be updated (Peake, 2022). Al effects on gas generation are not considered in the PA calculations (DOE, 2019c). Al will generate 1.5 mol of H_2 per mol of Al based on the three possible reactions of Al with water (Godart et al., 2019).
- Lead is another nonferrous metal present in the repository. In past PA calculations gas generation from lead was insignificant based on the Performance Assessment Inventory

Information Only

Report (PAIR). Since then, there has been an increase in the lead inventory, but due to the availability of some experimental lead corrosion data, the potential for gas generation has been re-evaluated and screened out of PA calculations for CRA-2019 (DOE, 2019a; Kirkes, 2019). The EPA position is to re-evaluate lead corrosion contributions to gas generation if lead inventory increases significantly (Peake, 2022). FEPs were reevaluated in (Kirkes, 2022; Kirkes & McCormick, 2023).

GEOCHEM-6.2 Expected Repository Conditions

Based on the chemical conditions conceptual model, the following conditions as they relate to Fe corrosion are expected in the repository (DOE, 2019a). When the shafts are sealed there will be an initial 100-year (approx.) oxic period, when oxygen is consumed by corrosion reactions and microbial processes. After that, anoxic conditions are expected to dominate in the repository (Brush, 1990; Brush, 1995; Roselle, 2013; Y. Wang & L. H. Brush, 1996). Anoxic corrosion of Fe can occur as soon as the shafts are sealed (assuming brine is available) and will produce H_2 gas. It is assumed that corrosion is a contributor to the total quantity of gas generated in the repository. Other contributing mechanisms include brine radiolysis and microbial respiration (DOE, 2019c, 2019e). Pressures are expected to increase due to corrosion reactions, microbial activity, radiolysis, and creep closure (self-healing properties of salt). The maximum pressure after closure is expected to be 15 MPa (~ 150 atm) (DOE, 2019a).

PA simulations predict that brine availability will be the corrosion limiting factor rather than availability of Fe (DOE, 2019d). Brine is expected to be Salado brine, Castile brine (Castile is a geological formation under the Salado formation where the repository is located) or a mixture of the two. Brine composition is assumed to be constant after initial equilibration with periclase (MgO). Equilibrium is assumed between repository brine, waste, and Salado minerals halite, anhydrite, brucite, and either hydromagnesite or magnesite. The MgO backfill will buffer the pH, which is expected to be between 8.8 and 10 (DOE, 2019a; Wilson et al., 1996). Cement material will contain calcium hydroxide $Ca(OH)_2$. $Ca(OH)_2$ which could react with magnesium chloride in brine to form calcium chloride, however the pH change is expected to be minimal.

The temperature (T) post-closure will remain at approximately 27°C (300 K) due to the high thermal conductivity of salt (DOE, 2019a). Heat generated from waste may temporarily (decades at most) increase the T by 12°C (Sanchez & Trellue, 1996; Y. Wang & L. H. Brush, 1996).

Redox equilibrium in the repository is not assumed (Wilson et al., 1996). Redox conditions are set by the corrosion of Fe. Fe corrosion is represented using reaction rates. As mentioned previously corrosion will reduce the oxidation state of some of the actinides and affect their solubility, binding constants, and therefore mobility. Expected oxidation states based on experimental data are, americium +3, thorium +4, plutonium +3 or +4, neptunium +4 or +5, and uranium +4 or +6 (DOE, 2019d).

Information Only

GEOCHEM-6.3 Corrosion Effects on Actinides

The linkages of Fe chemistry to redox chemistry are well established in the literature (Baes, 1953; Behrends & Van Cappellen, 2005; Farrell et al., 1999; Fredrickson et al., 2000; Huizenga & Magnusson, 1951; Nakata et al., 2004). Ferrous oxides, zero valent iron (ZVI or Fe metal), and aqueous ferrous Fe ($Fe(II)_{aq}$) will be present in reducing environments. Reduced Fe species will reduce higher-valent actinides in the WIPP, leading to lower actinide solubilities (Altmaier et al., 2009; DOE, 2019d; Felmy et al., 2011; Rai et al., 2002; Reed et al., 2006). ZVI and Fe(II) have been shown to quantitatively reduce Pu(VI) in WIPP brines to either Pu(IV) or Pu(III) (Reed et al., 2011; Reed et al., 2006). Recent studies suggest that Fe_3O_4 stoichiometry (stoichiometric magnetite is more reducing) can significantly influence the extent of U(VI) reduction (Latta et al., 2012). Neretnieks has shown that when dissolved actinides in moving groundwater came in contact with Fe(II), the actinides were reduced to a much-less-soluble oxidation state and precipitated (Neretnieks, 1983). The use of ZVI barriers has been reported for the removal of U(VI) from groundwater (Farrell et al., 1999; Fiedor et al., 1998; Gu et al., 1998). Dodge and O'Loughlin demonstrated that U(VI) is reduced to U(IV) by green rusts (Dodge et al., 2002; O'Loughlin et al., 2003). Green rust is one of the possible corrosion products in the repository. For details on these and additional interactions refer to appendix SOTERM (DOE, 2019d).

Information Only

GEOCHEM-7.0 Colloids

CRA-2019 Section GEOCHEM 7.0 provides an overview of the changes to colloid parameters for the next CRA.

GEOCHEM-7.1 Implementation of Colloidal Actinides in PA

In the WIPP PA, actinides may be mobilized as 1) dissolved species or 2) colloidal species. The actinide source term contains both (aqueous and colloidal) mobilized source terms constrained by concentration limits of actinide solid phases. The concentration of each actinide-associated colloid type is determined individually and added to the dissolved (non-colloidal) actinide source term to compute the total mobilization potential of each actinide. For inorganic colloids, a fixed concentration of the colloidally-bound actinide is added to the dissolved source term. For organic colloids, proportionality constants and upper limits on capacity are used.

Calculation of the total mobilization potential associated with colloids is described in Appendix-PA Section PA-4.4.1. Table GEOCHEM 15 lists WIPP colloid model parameters. Table GEOCHEM 16 lists CRA-2019 parameter values, and the next CRA recommended parameter values.

Table GEOCHEM 15: WIPP Colloid Model Parameter Summary

Material	Property	Brief Description of Parameter
Th, U, Np, Pu, Am	CONCMIN[a]	Concentration of actinide associated with mobile mineral fragment colloids
Th, U, Np, Pu, Am	CONCINT[a]	Concentration of actinide associated with mobile intrinsic actinide colloids
Th, U, Np, Pu, Am	PROPMIC[b]	Proportionality constant for concentration of actinides associated with mobile microbes
PHUMOX3 [c] PHUMOX4 PHUMOX5 PHUMOX6	PHUMCIM[b]	Proportionality constant for concentration of actinides associated with mobile humic colloids; in Castile brine; actinide solubilities include organics (complexes with organic ligands in the performance assessment repository inventory); solubilities were calculated assuming equilibrium with Mg-bearing minerals (brucite and hydromagnesite)
PHUMOX3 [c] PHUMOX4 PHUMOX5 PHUMOX6	PHUMSIM[b]	Proportionality constant for concentration of actinides associated with mobile humic colloids; in Salado brine; actinide solubilities include organics (complexes with organic ligands in the performance assessment repository inventory); solubilities were calculated assuming equilibrium with Mg-bearing minerals (brucite and hydromagnesite)

Information Only

Material	Property	Brief Description of Parameter
Th, U, Np, Pu, Am	CAPMIC[a]	Maximum (cap) concentration of actinide associated with mobile microbes
Th, U, Np, Pu, Am	CAPHUM[a]	Maximum (cap) concentration of actinide associated with mobile humic colloids

[a] In units of moles colloidal actinide per liter.

[b] In units of moles colloidal actinide per mole dissolved actinide.

[c] Proportionality constant for actinide concentrations associated with mobile humic substances for PHUMOX3, for actinide elements with oxidation state *III* (that is, Pu(III) and Am(III)); PHUMOX4, oxidation state IV (Th(IV), U(IV), Np(IV), and Pu(IV)); PHUMOX5, oxidation state V (Np(V)); and PHUMOX6, oxidation state VI (U(VI)).

Information Only

Table GEOCHEM 16: WIPP Colloid Parameter Values Estimated for Use in CRA-2019 (DOE, 2019b) and the next CRA

Recommended Oxidation State Specific Colloid Parameters for CRA-2019							
Actinide	**CONCMIN[a]**	**CONCINT[a]**	**PROPMIC[b]**	**CAPMIC[a]**	**PHUMSIM[b]**	**PHUMCIM[b]**	**CAPHUM[a]**
Th(IV)	2.6×10^{-8}	4.3×10^{-8}	0.21	3.8×10^{-8}	0.01	0.01	1.1×10^{-5}
U(IV)	2.6×10^{-8}	4.3×10^{-8}	0.21	3.8×10^{-8}	0.01	0.01	1.1×10^{-5}
U(VI)	2.6×10^{-8}	1.4×10^{-6}	ND[c]	3.8×10^{-8}	0.12	0.51	1.1×10^{-5}
Np(IV)	2.6×10^{-8}	4.3×10^{-8}	0.21	3.8×10^{-8}	0.01	0.01	1.1×10^{-5}
Np(V)	2.6×10^{-8}	ND[c]	ND[c]	3.8×10^{-8}	9.1×10^{-4}	7.4×10^{-3}	1.1×10^{-5}
Pu(III)	2.6×10^{-8}	9.5×10^{-9}	0.03	3.8×10^{-8}	0.2	0.2	1.1×10^{-5}
Pu(IV)	2.6×10^{-8}	4.3×10^{-8}	0.21	3.8×10^{-8}	0.01	0.01	1.1×10^{-5}
Am(III)	2.6×10^{-8}	9.5×10^{-9}	0.03	2.3×10^{-9}	0.2	0.2	1.1×10^{-5}
Recommended Oxidation State Specific Colloid Parameters for the next CRA							
Actinide	**CONCMIN[a]**	**CONCINT[a]**	**PROPMIC[b]**	**CAPMIC[a]**	**PHUMSIM[b]**	**PHUMCIM[b]**	**CAPHUM[a]**
Th(IV)	2.6×10^{-8}	4.8×10^{-7}	3.1	6.95×10^{-4}	0.01	0.01	1.1×10^{-5}
U(IV)	2.6×10^{-8}	4.3×10^{-8}	0.0021	2.22×10^{-6}	0.01	0.01	1.1×10^{-5}
U(VI)	2.6×10^{-8}	1.4×10^{-6}	ND[c]	ND[c]	0.12	0.51	1.1×10^{-5}
Np(IV)	2.6×10^{-8}	4.3×10^{-8}	12	2.33×10^{-6}	0.01	0.01	1.1×10^{-5}
Np(V)	2.6×10^{-8}	ND[c]	ND[c]	ND[c]	9.1×10^{-4}	7.4×10^{-3}	1.1×10^{-5}
Pu(III)	2.6×10^{-8}	4.3×10^{-8}	0.3	9.00×10^{-7}	0.8	0.9	1.1×10^{-5}
Pu(IV)	2.6×10^{-8}	4.3×10^{-8}	ND[c]	1.22×10^{-9}	0.01	0.01	1.1×10^{-5}
Am(III)	2.6×10^{-8}	6.7×10^{-7}	3.52	9.00×10^{-7}	0.8	0.9	1.1×10^{-5}

[a] In units of moles colloidal actinide per liter.

[b] In units of moles colloidal actinide per mole dissolved actinide.

[c] In PA calculations, for values listed as ND, the value of the lower oxidation-state of the same element were used.

Information Only

GEOCHEM-7.2 Changes Since CRA-2019

Changes to the colloid model parameters for CRA-2026 were driven by the EPA completeness comments after CRA-2019 (EPA, 2022) and new experimental data as discussed below.

GEOCHEM-7.2.1 Mineral Fragment Colloids

There are no changes to the mineral fragment parameter values for the next CRA. The element specific mineral fragment colloid parameters have remained unchanged since the CCA.

The EPA recommended that DOE evaluate the potential formation of actinide(IV)-silica colloids under WIPP conditions for future PA because of the presence of Si in waste soils, TRU waste, and in the repository horizon itself (EPA, 2022). To address the EPA concern, the effect of dissolved silica on the solubility of An(III) and An(IV) solids and the possibility of actinide-silica colloid formation in 5 M NaCl solutions were examined by (Beam, 2022). No significant colloidal fraction was observed by sequential filtration. Moreover, no measurable increase in An(III) and An(IV) solubility was observed in the presence of dissolved silica indicating that actinide-silica colloids are unlikely to form under conditions simulating a Direct Brine Release scenario (Beam, 2022; Lucchini & Swanson, 2023).

GEOCHEM-7.2.2 Intrinsic Colloids

The EPA, in its technical support document for the CRA-2019 (EPA, 2022), recommended the following two changes to the intrinsic colloid parameters:

1. Increase Am intrinsic colloid concentration to 6.7×10^{-7} M from 9.5×10^{-9} M
2. Increase Th intrinsic colloid concentration to 4.8×10^{-7} M from 4.3×10^{-8} M

These changes were based on 1) matching the upper bound concentration in long-term Am analogue Nd(III) solubility experiments (Borkowski et al., 2010; Reed et al., 2013) and 2) increased consistency with Th(IV) experimental data considered in the WIPP PA (Altmaier et al., 2004; Borkowski, 2012; Lucchini & Swanson, 2023). The DOE accepted the EPA recommended changes (Lucchini & Swanson, 2023). The new parameter values for the next CRA are listed in Table GEOCHEM 16.

GEOCHEM-7.2.3 Humic Substance Colloids

As a consequence of the EPA's recommendation to update the WIPP thermodynamic database, the EPA also recommended that the contribution of humic substance colloids be recalculated on the updated actinide solubility calculations following corrections to EDTA thermodynamic parameters in the WIPP thermodynamic database (EPA, 2022).

In response, DOE updated the humic colloid parameters to maintain consistency with the new DATA0.FM6 thermodynamic database (Domski, 2023c) and the revised baseline solubility calculations (Domski, 2023a). The updates to the parameters are described in (Mariner, 2023).

Information Only

GEOCHEM-7.2.4 Microbial Colloids

For the Microbial colloid parameters PROPMIC and CAPMIC, element-specific changes are recommended due to 1) the usage of only element-specific values in the PA and 2) that no new data for oxidation states other than An(III) have been generated since the CRA-2019 (Lucchini & Swanson, 2023). These parameter updates were implemented in the RPPCR and are discussed further below in the context of the next CRA.

The EPA, in its technical support document for the CRA-2019 recommended the use of CAPMIC parameter values (Peake, 2020) recalculated from CCA experiments (Papenguth, 1996), and that PROPMIC values be amended to be consistent with CCA values, unless new experimental data is produced.

The CAPMIC parameter values recommended for use in the next CRA are instead derived from CCA era filtration experiments described in (Francis et al., 1998). The use of these CAPMIC values rather than recalculated values from the experiments of (Papenguth, 1996) is motivated by the stricter adherence of the (Francis et al., 1998) study to the definition of CAPMIC (Lucchini & Swanson, 2023).

The PROPMIC parameter values recommended for use in the next CRA will follow the EPA recommendation to use CCA values, except for the values for Am(III) and Pu(III) for which new experimental data has been generated. The recommended PROPMIC value for the An(III)-oxidation state is based on the highest value obtained from recent WIPP-relevant experiments with *Halobacterium* sp. In ERDA-6 brine over a five-week experimental duration (Lucchini & Swanson, 2023; Swanson, 2022).

Information Only

GEOCHEM-8.0 References

Altmaier, M., Metz, V., Neck, V., Müller, R., & Fanghänel, T. (2003). Solid-liquid equilibria of Mg(OH)2(cr) and Mg2(OH)3Cl·4H2O(cr) in the system Mg-Na-H-OH-Cl-H2O at 25°C. *Geochimica et Cosmochimica Acta*, *67*(19), 3595-3601. https://doi.org/10.1016/s0016-7037(03)00165-0

Altmaier, M., Neck, V., & Fanghänel, T. (2004). Solubility and colloid formation of Th(IV) in concentrated NaCl and MgCl2solution. *RADIOCHIMICA ACTA*, *92*(9-11), 537-543. https://doi.org/10.1524/ract.92.9.537.54983

Altmaier, M., Neck, V., Lützenkirchen, J., & Fanghänel, T. (2009). Solubility of plutonium in $MgCl_2$ and $CaCl_2$ solutions in contact with metallic iron. *Radiochimica Acta*, *97*(4-5), 187-192. https://doi.org/doi:10.1524/ract.2009.1593

Associates), S. S. C. a. (2008). *Verification of the Waste Isolation Pilot Plant Chemistry Conceptual Models, Final Report*.

Baes, C. F., Jr. (1953). *The Reduction of Uranium(VI) by Ferrous Iron in Phosphoric Acid Solution: The Formal Electrode Potential of the U(IV)/(VI) Couple*.

Baes, C. F., & Mesmer, R. S. (1976). The Hydrolysis of Cations. *Berichte der Bunsengesellschaft für physikalische Chemie*, *81*(2), 245-246. https://doi.org/10.1002/bbpc.19770810252

Beam, J. C. (2022). *Actinide (III/IV) – Silica Colloids in the WIPP. Los Alamos National Laboratory report LCO-ACP-27, Revision 0. LA-UR-22-31798*.

Behrends, T., & Van Cappellen, P. (2005). Competition between enzymatic and abiotic reduction of uranium(VI) under iron reducing conditions. *Chemical Geology*, *220*(3), 315-327. https://doi.org/https://doi.org/10.1016/j.chemgeo.2005.04.007

Borkowski, M. (2012). Numerical Values for Graphs Presented in Report LCO-ACP-17 Entitled Solubility of An(IV) in WIPP Brine: Thorium Analog Studies in WIPP Simulated Brine, and for Graphs Published in Borkowski, M., et al., Carlsbad, NM: Los Alamos National Laboratory — Carlsbad Operations. Radiochimica Acta, (Revision 0). 98 (9-11), 577–582 (2010). LANL-CO ACRSP ACP-01/2012, LA-UR 12–26640.

Borkowski, M., Lucchini, J.-F., Richmann, M. K., & Reed, D. T. (2010). *Actinide (III) Solubility in WIPP Brine: Data Summary and Recommendations. Los Alamos National Laboratory; Carlsbad, NM. LA-UR-14360*.

Bruno, J., Wersin, P., & Stumm, W. (1992). On the influence of carbonate in mineral dissolution: II. The solubility of FeCO3 (s) at 25°C and 1 atm total pressure. *Geochimica et Cosmochimica Acta*, *56*(3), 1149-1155. https://doi.org/10.1016/0016-7037(92)90052-k

Brush, L. H. (1990). *Test Plan for Laboratory and Modeling Studies of Repository and Radionuclide Chemistry for the Waste Isolation Pilot Plant*.

Brush, L. H. (1995). *Systems Prioritization Method - Iteration 2 Baseline Position Paper: Gas Generation in the Waste Isolation Pilot Plant* (ERMS 228740).

Brush, L. H., & Domski, P. S. (2013). *Uncertainty Analysis of Actinide Solubilities for the WIPP CRA-2014 PA, Rev. 1, Supersedes ERMS 559278. Analysis report, February 22, 2013. Carlsbad, NM: Sandia National Laboratories. ERMS 559712*.

Information Only

Brush, L. H., Domski, P. S., & Xiong, Y.-L. (2012). *Analysis Plan for WIPP Near-Field Geochemical Process Modeling. AP-153, Rev. 1, February 8, 2012. Carlsbad, NM: Sandia National Laboratories. ERMS 556960.*

Brush, L. H., Xiong, Y.-L., Garner, J. W., Ismail, A., & Roselle, G. T. (2006). *Consumption of Carbon Dioxide by Precipitation of Carbonate Minerals Resulting from Dissolution of Sulfate Minerals in the Salado Formation In Response to Microbial Sulfate Reduction in the WIPP. Analysis report. Carlsbad, NM: Sandia National Laboratories. ERMS 544785.*

Clover, D., Kinsella, B., Pejcic, B., & De Marco, R. (2005). The influence of microstructure on the corrosion rate of various carbon steels. *Journal of Applied Electrochemistry, 35*(2), 139-149. https://doi.org/10.1007/s10800-004-6207-7

Deng, H., Xiong, Y., Nemer, M., & Johnsen, S. (2009). *Experimental Work Conducted on MgO Long-Term Hydration, Milestone Report. Carlsbad, NM: Sandia National Laboratories. ERMS 551421.*

Dodge, C. J., Francis, A. J., Gillow, J. B., Halada, G. P., Eng, C., & Clayton, C. R. (2002). Association of Uranium with Iron Oxides Typically Formed on Corroding Steel Surfaces. *Environmental Science & Technology, 36*(16), 3504-3511. https://doi.org/10.1021/es011450+

DOE, U. S. (1996a). *Title 40 CFR Part 191 Compliance Certification Application for the Waste Isolation Pilot Plant, Vol. 1-21.* (DOE/CAO-1994-2184). Carlsbad, NM: U.S. Department of Energy Carlsbad Area Office

DOE, U. S. (1996b). *Title 40 CFR Part 191 Subparts B and C Compliance Recertification Application 1996 for the Waste Isolation Pilot Plant, Appendix SOTERM, SOTERM.6.*

DOE, U. S. (2004). *Title 40 CFR Part 191 Compliance Recertification Application for the Waste Isolation Pilot Plant, Vol. 1-8.* (DOE/WIPP 2004-3231). Carlsbad, NM: U.S. Department of Energy Carlsbad Field Office

DOE, U. S. (2014). *Title 40 CFR Part 191 Subparts B and C Compliance Recertification Application 2014 for the Waste Isolation Pilot Plant, Appendix MgO-2014. Magnesium Oxide as an Engineered Barrier.*

DOE, U. S. (2019a). *Title 40 CFR Part 191 Subparts B and C Compliance Recertification Application 2019 for the Waste Isolation Pilot Plant, Appendix GEOCHEM-2019, Implementation of Chemistry Conceptual Models* (DOE/WIPP-19-3609, Rev. 0).

DOE, U. S. (2019b). *Title 40 CFR Part 191 Subparts B and C Compliance Recertification Application 2019 for the Waste Isolation Pilot Plant, Appendix PA-2019, Performance Assessment.*

DOE, U. S. (2019c). *Title 40 CFR Part 191 Subparts B and C Compliance Recertification Application 2019 for the Waste Isolation Pilot Plant, Appendix SCR-2019, Feature, Event, and Process Screening for PA. Carlsbad Field Office, Carlsbad, NM. DOE/WIPP-19-3609, Rev. 0.*

DOE, U. S. (2019d). *Title 40 CFR Part 191 Subparts B and C Compliance Recertification Application 2019 for the Waste Isolation Pilot Plant, Appendix SOTERM-2019, Actinide Chemistry Source Term* (DOE/WIPP-19-3609, Rev. 0).

DOE, U. S. (2019e). *Title 40 CFR Part 191 Subparts B and C Compliance Recertification Application 2019 for the Waste Isolation Pilot Plant, Appendix SOTERM-2019, Actinide Chemistry Source Term. Carlsbad Field Office, Carlsbad, NM. DOE/WIPP-19-3609, Rev. 0.*

Information Only

Domski, P. S. (2019a). *Official Release of the Qualified Pitzer Thermodynamic Database, DATA0.FM4, for EQ3/6 under AP-183, Revision 1. Carlsbad, NM: Sandia National Laboratories. ERMS 571051.*

Domski, P. S. (2019b). *Uncertainty Analysis of Actinide Solubilities for CRA 2019. Sandia National Laboratories, Carlsbad, New Mexico. ERMS 571179.*

Domski, P. S. (2022). *EPA Issue 23: Implementation of the Neck et al. (2009) Am(III) Model. Memorandum to WIPP Records, July 21, 2022. Carlsbad, NM: Sandia National Laboratories. ERMS 577677.*

Domski, P. S. (2023a). *Prediction of Baseline Actinide Solubilities for the Replacement Panels Planned Change Request (RPPCR) Performance Assessment. Carlsbad, NM: Sandia National Laboratories. ERMS 579503.*

Domski, P. S. (2023b). *Uncertainty Analysis of Actinide Solubilities for the Replacement Panels Planned Change Request (RPPCR) Performance Assessment and the 2024 Compliance Recertification Application (CRA-2024). Carlsbad, NM: Sandia National Laboratories. ERMS 579525.*

Domski, P. S. (2023c). *An Update to the WIPP EQ3/6 Database DATA0.FM1 with the Creation of DATA0.FM6. Carlsbad, NM: Sandia National Laboratories. ERMS 579370.*

Domski, P. S., & Nemer, M. (2023a). *On the Occurrence and Solubility of the Magnesium Hydroxy-Chloride Phases: Phase 3 and Phase 5 in the WIPP Near-Field Environment. Memorandum to WIPP Records, March 2, 2023. Carlsbad, NM: Sandia National Laboratories. SAND2023-012630.*

Domski, P. S., & Nemer, M. (2023b). *Revised Literature Screening Criteria for the WIPP Actinide Solubility Uncertainty Analysis, Revision 1. Carlsbad, NM: Sandia National Laboratories. SAND2023-01264O.*

Domski, P. S., & Sisk-Scott, C. (2019). *Prediction of Baseline Actinide Solubilities for CRA 2019 with and Updated EQ3/6 Pitzer Thermodynamic Database, DATA0.FM4. Carlsbad, NM: Sandia National Laboratories. ERMS 571178.*

Dosch, R. G., & Lynch, A. W. (1978). *Interaction of Radionuclides with Geomedia Associated with the Waste Isolation Pilot Plant (WIPP) Site in New Mexico, Department of Energy, Sandia Laboratories.* https://books.google.com/books?id=v_bLvAEACAAJ

Edwards, R., Gillard, R. D., Williams, P. A., & Pollard, A. M. (1992). Studies of Secondary Mineral Formation in the PbO-H2O-HCl System. *Mineralogical Magazine*, *56*(282), 53-65. https://doi.org/http://10.1180/minmag.1992.056.382.06

EPA, U. S. (2008). *Verification of the Waste Isolation Pilot Plant Chemistry Conceptual Models.* U. S. E. P. Agency.

EPA, U. S. (2017). *Technical Support Document for Section 194.24: Evaluation of the Compliance Recertification Actinide Source Term, Backfill Efficacy and Culebra Dolomite Distribution Coefficient Values* (DOCKET: EPA-HQ-OAR-2014-0609).

EPA, U. S. (2019). *Technical Support Document for Section 194.24: Evaluation of the Compliance Recertification – Actinide Source Term Gas Generation, Backfill Efficacy, Water Balance, And Culebra Dolomite Distribution Coefficient Values. Washington, DC. EPA DOCKET: EPA-HQ-OAR-2019-0534.*

Information Only

EPA, U. S. (2022). *Technical Support Document for Section 194.24: Evaluation of the Compliance Recertification – Actinide Source Term Gas Generation, Backfill Efficacy, Water Balance, And Culebra Dolomite Distribution Coefficient Values. Washington, DC.* .

Farrell, J., Bostick, W. D., Jarabek, R. J., & Fiedor, J. N. (1999). Uranium Removal from Ground Water Using Zero Valent Iron Media. *Groundwater*, *37*(4), 618-624. https://doi.org/https://doi.org/10.1111/j.1745-6584.1999.tb01150.x

Felmy, A. R., Moore, D. A., Rosso, K. M., Qafoku, O., Rai, D., Buck, E. C., & Ilton, E. S. (2011). Heterogeneous Reduction of PuO_2 with Fe(II): Importance of the Fe(III) Reaction Product. *Environmental Science & Technology*, *45*(9), 3952-3958. https://doi.org/10.1021/es104212g

Fiedor, J. N., Bostick, W. D., Jarabek, R. J., & Farrell, J. (1998). Understanding the Mechanism of Uranium Removal from Groundwater by Zero-Valent Iron Using X-ray Photoelectron Spectroscopy. *Environmental Science & Technology*, *32*(10), 1466-1473. https://doi.org/10.1021/es970385u

Folkman, Y., & Wachs, A. M. (1973). Removal of algae from stabilization pond effluents by lime treatment. *WATER RESEARCH*, *7*(3), 419-435. https://doi.org/https://doi.org/10.1016/0043-1354(73)90024-9

Francis, A. J., Gillow, J. B., Dodge, C. J., Dunn, M. K., Mantione, K., Strietelmeier, B. A., PansoyHjelvik, M. E., & Papenguth, H. W. (1998). Role of Bacteria as Biocolloids in the Transport of Actinides from a Deep Underground Radioactive Waste Repository. Radiochimica Acta 82: 347-354.

Fredrickson, J. K., Zachara, J. M., Kennedy, D. W., Duff, M. C., Gorby, Y. A., Li, S.-m. W., & Krupka, K. M. (2000). Reduction of U(VI) in goethite (α-FeOOH) suspensions by a dissimilatory metal-reducing bacterium. *Geochimica et Cosmochimica Acta*, *64*(18), 3085-3098. https://doi.org/https://doi.org/10.1016/S0016-7037(00)00397-5

Godart, P., Fischman, J., Seto, K., & Hart, D. (2019). Hydrogen production from aluminum-water reactions subject to varied pressures and temperatures. *International Journal of Hydrogen Energy*, *44*(23), 11448-11458. https://doi.org/https://doi.org/10.1016/j.ijhydene.2019.03.140

Gu, B., Liang, L., Dickey, M. J., Yin, X., & Dai, S. (1998). Reductive Precipitation of Uranium(VI) by Zero-Valent Iron. *Environmental Science & Technology*, *32*(21), 3366-3373. https://doi.org/10.1021/es980010o

Guillaumont, R., Fanghanel, T., Fuger, J., Grenthe, I., Neck, V., Palmer, D. A., & Rand, M. H. (2003). *Update on the chemical thermodynamics of uranium, neptunium, plutonium, americium and technetium* (Vol. 5). Elsevier Amsterdam.

Guo, J., Yang, S., Shang, C., Wang, Y., & He, X. (2009). Influence of carbon content and microstructure on corrosion behaviour of low alloy steels in a Cl^- containing environment. *Corrosion Science*, *51*(2), 242-251. https://doi.org/https://doi.org/10.1016/j.corsci.2008.10.025

Haberman, J. H., & Frydrych, D. J. (1988). Corrosion Studies of A216 Grade WCA Steel in Hydrothermal Magnesium-Containing Brines. In M. J. A. a. R. E. Westerman, Materials Research Society Symposium Proceedings: Scientific Basis for Nuclear Waste Management XI, Pittsburgh.

Information Only

Huizenga, J. R., & Magnusson, L. B. (1951). Oxidation-Reduction Reactions of Neptunium(IV) and (V). *Journal of the American Chemical Society, 73*(7), 3202-3206. https://doi.org/10.1021/ja01151a061

Hummel, W., Anderegg, G., Puigdomènech, I., Rao, L., & Tochiyama, O. (2005). *Chemical Thermodynamics of Compounds and Complexes of: U, Np, Pu, Am, Tc, Zr, Ni and Se with Selected Organic Ligands* (Vol. 9). Elsevier.

Jang, J. (2020). *Experimental Study of the Thermodynamic Equilibrium Constants for the Magnesium - Oxalate Systems using Pitzer Activity Model, Revision 0. GEOC-19-05. Sandia National Laboratories, Carlsbad, NM, ERMS 573285.*

Jang, J. (2021). *Revisit to the Pitzer Geochemical Thermodynamic Model for the PbCl2(s)-HCl-H2O System. Sandia National Laboratories, Carlsbad, NM, ERMS 575309.*

Jang, J. (2022). *The PbCO3(s) - NaHCO3 - Na2CO3 - H2O Experiment (Revision 0): Addendum to Xiong (2015a,b). Memo to SNL WIPP Records Center and SNL WIPP Geochemistry. Sandia National Laboratories, Carlsbad, NM, ERMS 578642.*

Jang, J. (2023a). *The PbSO4(s) - Na2SO4 - NaCl - H2O Experiment (Revision 0). Memo to SNL WIPP Records Center, SNL WIPP Geochemistry. Sandia National Laboratories, Carlsbad, NM, ERMS 578721.*

Jang, J. (2023b). *Thermodynamic quantities for Fe+2 - SO4-2 - H+ - H2O system (Revision 0). Memo to SNL WIPP Records Center, SNL WIPP Geochemistry. Sandia National Laboratories, Carlsbad, NM, ERMS 578717.*

Jang, J., & Foil, I. (2023). *GEOC-22-01: Solubility and Complexation of Iron, Lead, Magnesium, Neodymium, Boron, and Calcium in Brines, Revision 1 of GEOC-21-11. Sandia National Laboratories, Carlsbad, NM, ERMS 578806.*

Jang, J., Hora, P., Kirkes, L., Miller, C., & Zhang, L. (2021). *Analysis Report documenting Solubility and Complexation of Iron, Lead, Magnesium, Neodymium, and Boron in the WIPP-Relevant Brines under TPs 06-03, 08-02, 12-02, 14-03, 14-05, 16-02, 19-01, and 20-01. Revision 0. Sandia National Laboratories. GEOC-21-11. ERMS 576381. SAND2022-13723R.* [4]

Jaouhari, R., Benbachir, A., Guenbour, A., Gabrielli, C., Garcia-Jareno, J., & Maurin, G. (2000). Influence of water composition and substrate on electrochemical scaling. *JOURNAL OF THE ELECTROCHEMICAL SOCIETY, 147*(6), 2151.

Katz, J. L., Reick, M. R., Herzog, R. E., & Parsiegla, K. I. (1993). Calcite growth inhibition by iron. *Langmuir, 9*(5), 1423-1430.

Kim, S., Marrs, C., Nemer, M., & Jang, J. (2017). *Solubility Model for Ferrous Iron Hydroxide, Hibbingite, Siderite, and Chukanovite in High Saline Solutions of Sodium Chloride, Sodium Sulfate, and Sodium Carbonate. Sandia National Laboratories, Carlsbad, NM. ERMS 569090.*

[4] Typographical error corrected in Domski, P. S., 2023. Memo of Correction: Transcription Error of $\beta^{(0)}$ value for the Mg^{2+} - $PbCl_3^-$ Binary Pitzer Parameter in GEOC 21-11. Sandia National Laboratories, Carlsbad, New Mexico, U.S.A. ERMS 579289.

Information Only

King, S. (2021). *Repository volume, DRZ volume, and minimum brine volume for a direct brine release for a repository with new panels. Sandia National Laboratories, Carlsbad, NM. ERMS 576475.*

Kirkes, L. (2019). *Lead Inventory Impact on Gas Generation* (ERMS 571255).

Kirkes, R. (2022). *AP-199 Analysis Plan for the Reassessment of Features, Events, and Processes for the 2024 Compliance Recertification Application. ERMS 578587.*

Kirkes, R., & McCormick, J. (2023). *Analysis report for the Reassessment of Features, Events, and Processes for the 2024 Compliance Recertification Application. ERMS 580866.*

Knerr, M. (2021). *Letter to Ms. Lee Ann B. Veal, Radiation Protection Division. Subject: Supplementary Information as Requested by U.S. Environmental Protection Agency During technical Exchange Meeting on June 22, 2020. Enclosure 1 Geochem Supplement – 1 for CRA 2019. July 8, 2021. U.S. Department of Energy, Carlsbad Field Office, Carlsbad, NM. Letter #21-0236.*

Knerr, R. (2021). *Response 12 to U.S. Environmental Protection Agency's 2019 Compliance Recertification Application Completeness Comments Letter dated September 11, 2020, from Tom Peake to Mike Brown. U.S. Department of Energy, Carlsbad Field Office, Carlsbad, New Mexico. Letter to L.B. Veal.* Washington, D.C.: U.S. Environmental Protection Agency Radiation Protection Division

Könnecke, T., Fanghänel, T., & Kim, J. (1997). Thermodynamics of trivalent actinides in concentrated electrolyte solutions: modelling the chloride complexation of Cm (III). *RADIOCHIMICA ACTA, 76*(3), 131-136.

Krumhansl, J. L., Kimball, K. M., & Stein, C. L. (1991). *Intergranular Fluid Compositions from the Waste Isolation Pilot Plant (WIPP), Southeastern New Mexico, Sandia National Laboratories. SAND90-0584.*

Latta, D. E., Gorski, C. A., Boyanov, M. I., O'Loughlin, E. J., Kemner, K. M., & Scherer, M. M. (2012). Influence of Magnetite Stoichiometry on UVI Reduction. *Environmental Science & Technology, 46*(2), 778-786. https://doi.org/10.1021/es2024912

Lemire, R., Berner, U., Musikas, C., Palmer, D., Taylor, P., Tochiyama, O., & Perrone, J. (2013). Chemical thermodynamics of iron-Part 1-Chemical thermodynamics volume 13a; Data Bank, Organisation for Economic Co-Operation and Development. *Nuclear Energy Agency, 13a.*

Liu, R., Cui, Y., Liu, L., & Wang, F. H. (2021). Study on the mechanism of hydrostatic pressure promoting electrochemical corrosion of pure iron in 3.5% NaCl solution [Article]. *Acta Materialia, 203*, 11. https://doi.org/10.1016/j.actamat.2020.11.009

Lucchini, J., & Swanson, J. S. (2023). *LANL ACRSP Parameter Recommendations for CRA-2024 Performance Assessment. Carlsbad, NM: Los Alamos National Laboratory. LCO-ACP-34, Revision 0. ERMS 57960.*

Mariner, P. E. (2023). *Updates to the WIPP humic Colloids models for An(III) and An(IV). July 26, 2023. Albuquerque, NM: Sandia National Laboratories. ERMS 580251. *.*

Martell, A. E. a. S., R. M. (1977). *Critical stability constants, Volume 3: Other Organic Ligands.* Plenum Press.

Miller, C., Domski, P. S., Jang, J., Rhino, K., & Nemer, M. (2022). *EPA Technical Exchange: Thermodynamic Database Issue Resolution. Sandia National Laboratories, Carlsbad, NM. SAND2022-14863C.*

Information Only

Millero, F. J., & Byrne, R. H. (1984). Use of Pitzer's equations to determine the media effect on the formation of lead chloro complexes. *Geochimica et Cosmochimica Acta*, *48*(5), 1145-1150.

Moog, H. C., Hagemann, S., & Rumyantsev, A. V. (2004). Isopiestic Investigation of the Systems FeCl2–(Na, K, Mg, Ca) Cl n–H2O at 298.15 K. *Zeitschrift für Physikalische Chemie-International Journal of Research in Physical Chemistry & Chemical Physics*, *218*(9), 1063-1087.

Morel, F. M. M., & Hering, J. G. (1993). *Principles and Applications of Aqueous Chemistry*. John Wiley & Sons.

Nakata, K., Nagasaki, S., Tanaka, S., Sakamoto, Y., Tanaka, T., & Ogawa, H. (2004). Reduction rate of neptunium(V) in heterogeneous solution with magnetite. *92*(3), 145-150. https://doi.org/doi:10.1524/ract.92.3.145.30493 (Radiochimica Acta)

Neck, V., Altmaier, M., Rabung, T., Lützenkirchen, J., & Fanghänel, T. (2009). Thermodynamics of trivalent actinides and neodymium in NaCl, MgCl2, and CaCl2 solutions: Solubility, hydrolysis, and ternary Ca-M (III)-OH complexes. *Pure and Applied Chemistry*, *81*(9), 1555-1568.

Nemer, M. B., Xiong, Y., Ismail, A. E., & Jang, J.-H. (2011). Solubility of $Fe_2(OH)_3Cl$ (pure-iron end-member of hibbingite) in NaCl and Na_2SO_4 brines. *Chemical Geology*, *280*(1), 26-32. https://doi.org/https://doi.org/10.1016/j.chemgeo.2010.10.003

Neretnieks, I. (1983). The Movement of a Redox Front Downstream from a Repository For Nuclear Waste. *Nuclear Technology*, *62*(1), 110-115. https://doi.org/10.13182/NT83-A33238

O'Loughlin, E. J., Kelly, S. D., Cook, R. E., Csencsits, R., & Kemner, K. M. (2003). Reduction of Uranium(VI) by Mixed Iron(II)/Iron(III) Hydroxide (Green Rust): Formation of UO_2 Nanoparticles. *Environmental Science & Technology*, *37*(4), 721-727. https://doi.org/10.1021/es0208409

Oakes, C. S., Ward, A. L., Chugunov, N., & Icenhower, J. (2021). A speciated, conventional Pitzer ion-interaction model for the aqueous Nd3+–H+–Na+–K+–Ca2+–Cl−–OH− system at 298 K and 0.1 MPa. *Geochimica et Cosmochimica Acta*, *297*, 308-327.

Odziemkowski, M. S., Schuhmacher, T. T., Gillham, R. W., & Reardon, E. J. (1998). Mechanism of oxide film formation on iron in simulating groundwater solutions: Raman spectroscopic studies. *Corrosion Science*, *40*(2), 371-389. https://doi.org/https://doi.org/10.1016/S0010-938X(97)00141-8

Pannach, M., Bette, S., & Freyer, D. (2017). Solubility equilibria in the system Mg (OH) 2–MgCl2–H2O from 298 to 393 K. *Journal of Chemical & Engineering Data*, *62*(4), 1384-1396.

Papenguth, H. W. (1996). *Letter to Christine T. Stockman. Subject: Parameter Record Package for Colloidal Actinide Source Term Parameters, Attachment A: Rationale for Definition of Parameter Values for Microbes. 7 May 1996. Sandia National Laboratories; Carlsbad, NM. ERMS 416348.*

Pavitt, A. (2024). *WIPP Steel Elemental Composition, ERMS 581242.*

Peake, T. (2018). *Letter to Mike Brown "2018-12-17 E Letter to CBFO WIPP Issues Summary".* U.S. Environmental Protection Agency, Center for Waste Management and Regulations

Information Only

Peake, T. (2020). *Letter to Mike Brown "Second Set of EPA Completeness Comments and Questions for CRA-2019"*. U.S. Environmental Protection Agency, Center for Waste Management and Regulations

Peake, T. (2022). *Letter to Michael Gerle "CRA-2019 Issues Table"*.

Popielak, R. S., Beauheim, R. L., Black, S. R., Coons, W. E., Ellingson, C. T., & Olsen, R. L. (1983). *Brine Reservoirs in the Castile Formation, Waste Isolation Pilot Plant Project, Southeastern New Mexico.*

Powell, K. J., Brown, P. L., Byrne, R. H., Gajda, T., Hefter, G., Leuz, A.-K., Sjöberg, S., & Wanner, H. (2009). Chemical speciation of environmentally significant metals with inorganic ligands. Part 3: The Pb2++ OH–, Cl–, CO32–, SO42–, and PO43–systems (IUPAC Technical Report). *Pure and Applied Chemistry*, *81*(12), 2425-2476.

Qiu, J., Wu, A., Li, Y., Xu, Y., Scarlat, R., & Macdonald, D. D. (2020). Galvanic corrosion of Type 316L stainless steel and graphite in molten fluoride salt. *Corrosion Science*, *170*, 108677. https://doi.org/https://doi.org/10.1016/j.corsci.2020.108677

Rai, D., Gorby, Y. A., Fredrickson, J. K., Moore, D. A., & Yui, M. (2002). Reductive Dissolution of PuO_2(am): The Effect of Fe(II) and Hydroquinone. *Journal of Solution Chemistry*, *31*(6), 433-453. https://doi.org/10.1023/A:1020200911842

Reardon, E., & Beckie, R. (1987). Modelling chemical equilibria of acid mine-drainage: The FeSO4-H2SO4-H2O system. *Geochimica et Cosmochimica Acta*, *51*(9), 2355-2368.

Reed, D. T., Borkowski, M., Swanson, J. S., Richmann, M. K., Khaing, H. Y., & Lucchini, J.-F. (2011). Redox-Controlling Processes for Multivalent Metals and Actinides in the WIPP. ReCosy, Roussillon, France.

Reed, D. T., Lucchini, J. F., Aase, S. B., & Kropf, A. J. (2006). Reduction of plutonium(VI) in brine under subsurface conditions. *Radiochimica Acta*, *94*(9-11), 591-597. https://doi.org/doi:10.1524/ract.2006.94.9-11.591 (Radiochimica Acta)

Reed, D. T., Swanson, J. S., Lucchini, J.-F., & Richmann, M. K. (2013). *Intrinsic, Mineral, and Microbial Colloid Enhancement Parameters for the WIPP Actinide Source Term. Carlsbad, NM: Los Alamos National Laboratory. LCO-ACP-18, LA-UR-13-20858.*

Roselle, G. T. (2009). *Iron and Lead Corrosion in WIPP-Relevant Conditions: Six Month Results* [Milestone Report](ERMS 552218).

Roselle, G. T. (2010). *Iron and Lead Corrosion in WIPP-Relevant Conditions: 12 Month Results* [Milestone Report](ERMS 554383).

Roselle, G. T. (2011a). *Iron and Lead Corrosion in WIPP-Relevant Conditions: 18 Month Results* [Milestone Report](ERMS 554715).

Roselle, G. T. (2011b). *Iron and Lead Corrosion in WIPP-Relevant Conditions: 24 Month Results* [Milestone Report](ERMS 555426).

Roselle, G. T. (2013). *Determination of Corrosion Rates from Iron/Lead Corrosion Experiments to be used for Gas Generation Calculations (Revision 1)* [Analysis Report](ERMS 559077).

Sanchez, L. C., & Trellue, H. R. (1996). Memorandum to T. Hicks. Subject: Estimation of Maximum RH-TRU Thermal Heat Load for WIPP. In. Albuquerque, NM: Sandia National Laboratories.

Schikorr, G. (1933). Über Eisen(II)-hydroxyd und ein ferromagnetisches Eisen(III)-hydroxyd. *Zeitschrift für anorganische und allgemeine Chemie*, *212*(1), 33-39. https://doi.org/https://doi.org/10.1002/zaac.19332120105

Information Only

Shock, E. L., Sassani, D. C., Willis, M., & Sverjensky, D. A. (1997). Inorganic species in geologic fluids: correlations among standard molal thermodynamic properties of aqueous ions and hydroxide complexes. *Geochimica et Cosmochimica Acta*, *61*(5), 907-950.

Sisk-Scott, C. (2019a). *Analysis Plan to Update the WIPP Geochemical Thermodynamic Database (DATA0.FM1) to Data0.FM4 for CRA-2019. AP-183, Revision 1. Sandia National Laboratories, Carlsbad, NM. ERMS 571001.*

Sisk-Scott, C. (2019b). *Milestone Report for Iron and Lead Corrosion in WIPP-Relevant Conditions: Static and Solution Flow-Through Corrosion Experiments* (ERMS 572066).

Smart, N. R., Blackwood, D. J., & Werme, L. (2001). *The anaerobic corrosion of carbon steel and cast iron in artificial groundwaters* (SKB-TR-01-22).

Smith, B. T., & Davis, R. H. (2012). Sedimentation of algae flocculated using naturally-available, magnesium-based flocculants. *Algal Research*, *1*(1), 32-39. https://doi.org/https://doi.org/10.1016/j.algal.2011.12.002

Snider, A. C. (2003). *Verification of the Definition of Generic Weep Brine and the Development of a Recipe for This Brine. Analysis report. Sandia National Laboratories, Carlsbad, NM. ERMS 527505.*

Stein, C. L. (1985). *Mineralogy in the Waste Isolation Pilot Plant (WIPP) Facility Stratigraphic Horizon. Sandia National Laboratories, Albuquerque, NM. SAND-85-0321.*

Stumm, W., & Morgan, J. J. (1996). *Aquatic Chemistry, 3rd ed.* John Wiley and Sons.

Sun, H. J., Liu, L., Li, Y., & Wang, F. H. (2013). Effect of Hydrostatic Pressure on the Corrosion Behavior of a Low Alloy Steel. *Journal of the Electrochemical Society*, *160*(3), C89-C96. https://doi.org/10.1149/2.040303jes

Swanson, J. S. (2022). *Biologically Influenced Transport of the +3 Actinide Oxidation State from the WIPP Environment, Using Neodymium as an Analog. Los Alamos National Laboratory report LCO-ACP-32, Revision 0,LA-UR-22-32936.*.*

Telander, M. R., & Westerman, R. E. (1993). *Hydrogen generation by metal corrosion in simulated Waste Isolation Pilot Plant environments: Progress report for the period November 1989 through December 1992* (SAND92-7347).

Telander, M. R., & Westerman, R. E. (1997). *Hydrogen generation by metal corrosion in simulated Waste Isolation Pilot Plant environments* (SAND96-2538).

Van Soest, G. D. (2022). *Performance Assessment Inventory Report – 2022. INV-PA-2022, Revision 0. Carlsbad, NM: Los Alamos National Laboratory.*

Wall, N. A., & Mathews, S. A. (2005). Sustainability of humic acids in the presence of magnesium oxide. *APPLIED GEOCHEMISTRY*, *20*(9), 1704-1713. https://doi.org/https://doi.org/10.1016/j.apgeochem.2005.04.004

Wang, Y., & Brush, L. H. (1996). *Memorandum to M. S. Tierney. Subject: Estimates of Gas-Generation Parameters for the Long-Term WIPP Performance Assessment. In. Carlsbad, NM: Sandia National Laboratories.*

Wang, Y., & Brush, L. H. (1996). Memorandum to M. S. Tierney. Subject: Estimates of Gas-Generation Paramteres for the Long-Term WIPP Performance Assessement. In. Carlsbad, NM: Sandia National Laboratories.

Wilson, C., Porter, D., Gibbons, J., Oswald, E., Sjoblom, G., & Caporuscio, F. (1996). *Conceptual Models Supplementary Peer Review Report (December).*

Information Only

WIPP. (2023, 11/09/2023). *National TRU Programs - Controlled Documents*. Retrieved 11/20/2023 from https://www.wipp.energy.gov/ntpxport/

Wolery, T. W., & Jarek, R. L. (2003). *Software User's Manual: EQ3/6, Version 8.0. Sandia National Laboratories, Albuquerque, NM. 10813-UM-8.0-00*

Wolery, T. W., Xiong, Y.-L., & Long, J. J. (2011). *Verification and Validation Plan/Validation Document for EQ3/6 Version 8.0a for Actinide Chemistry, Document Version 8.20. Sandia National Laboratories, Carlsbad, NM. ERMS 555358*.

Xiong, Y., Deng, H., Nemer, M., & Johnsen, S. (2010). Experimental determination of the solubility constant for magnesium chloride hydroxide hydrate (Mg3Cl (OH) 5· 4H2O, phase 5) at room temperature, and its importance to nuclear waste isolation in geological repositories in salt formations. *Geochimica et Cosmochimica Acta*, *74*(16), 4605-4611.

Xiong, Y., Kirkes, L., & Marrs, C. (2017). Long-term experimental determination of solubilities of micro-crystalline Nd (III) hydroxide in high ionic strength solutions: applications to nuclear waste management. *Aquatic Geochemistry*, *23*, 359-375. [5]

Xiong, Y., & Lord, A. S. (2008). Experimental investigations of the reaction path in the MgO–CO2–H2O system in solutions with various ionic strengths, and their applications to nuclear waste isolation. *APPLIED GEOCHEMISTRY*, *23*(6), 1634-1659.

Young, P., Phasey, J., Wallis, I., Vandamme, D., & Fallowfield, H. (2021). Autoflocculation of microalgae, via magnesium hydroxide precipitation, in a high rate algal pond treating municipal wastewater in the South Australian Riverland. *Algal Research*, *59*, 102418. https://doi.org/https://doi.org/10.1016/j.algal.2021.102418

Zhu, T., Wang, L., Sun, W., Wang, M., Yang, Z., Ji, T., Wang, S., Wang, Y., Xia, L., & Liu, G. (2018). Origin of aragonite scale deposition on carbon steel at ambient circumstances. *Industrial & Engineering Chemistry Research*, *57*(1), 401-413.

[5] An addendum is provided in Jang, J., 2022. The $Nd(OH)_3(s)$ - NaCl - H_2O Experiment (Revision 0): Addendum to Xiong et al. (2016, 2017). Memo to SNL WIPP Records Center, SNL WIPP Geochemistry. September 26, 2022. Sandia National Laboratories, Carlsbad, New Mexico, U.S.A. ERMS 577978.

Information Only

GEOCHEM-9.0 Appendix

GEOCHEM-9.1 Comparison of Amendments in Appendix GEOCHEM-2019 towards GEOC-23-10

The latest version of the "Title 40 CFR Part 191 Subparts B and C Compliance Recertification Application 2019 for the Waste Isolation Pilot Plant Appendix GEOCHEM-2019 Implementation of Chemistry Conceptual Models," denoted as GEOC-23-10, underwent several comprehensive stages as shown in Figure GEOCHEM 9.

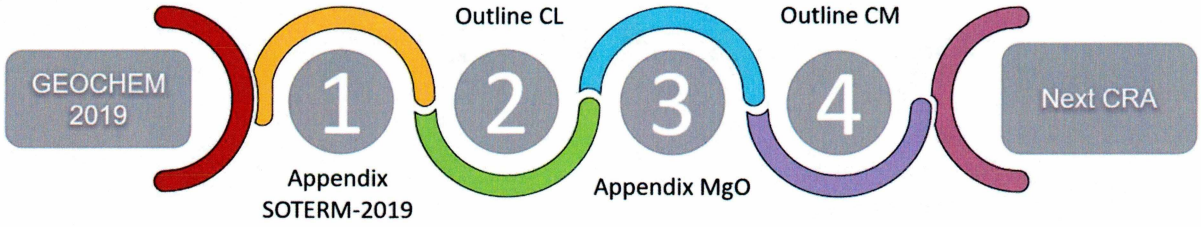

Figure GEOCHEM 9: Evolution of changes between GEOCHEM-2019 to GEOC-23-10.

Initially, the revision process involved a detailed comparison with Appendix SOTERM-2019. This scrutiny identified various areas of overlap, prompting the removal or revision of specific topics within the new GEOC-23-10 (see Table GEOCHEM 17 below). Elements such as Ambient Geochemistry/Repository Conditions, Repository Conditions, Temperature, Humidity, Water Content, Pressure, Brine Volume, Waste Characteristics/Inventory, Gas Phase/Production, Microbial Activity, Radiolysis, Dissolution and Dissociation Terms, Colloids, and Actinide Source Term were either removed or extensively revised.

Subsequently, a comparative analysis was conducted against an outline proposed by CL (Christi Leigh). This examination revealed that Appendix GEOCHEM-2019, consisting of five sections (excluding the References section), redistributed and reorganized the content of seven sections from the Leigh outline into its five sections. Notably, four of these sections connected the conceptual models with related process models, baseline solubility, uncertainty analysis, and colloid discussions throughout the document rather than summarizing them into dedicated sections.

Furthermore, a comparison with Appendix MgO-2024 resulted in the removal of overlapping elements. Appendix MgO-2024 primarily concentrates on operational aspects such as emplacement, excess factor selection, buffering, and is not directly linked to model parameterizations. The relationship between Appendices MgO-2024, GEOC-23-10, and SOTERM-2024 is established, with future opportunities highlighted to enhance Appendix MgO-2024 with uncertainty-amended measurements derived from GEOC-23-10 regarding rates and products of MgO hydration and carbonation.

Information Only

Additionally, GEOC-23-10 offers revised information on MgO. Active referencing of Appendix GEOCHEM-2019 and Appendix SOTERM-2019 elucidates the details concerning mineralogical transformation of MgO and its implications on chemical conditions and dissolved actinide source terms.

Finally, the document underwent adaptation to the CM (Chammi Miller) outline (see GEOCHEM 9.2), akin to the Leigh outline (2018).

Table GEOCHEM 17: Comparison GEOCHEM-2019 with SOTERM-2019

Topics	GEOCHEM-2019 Section	SOTERM-2019 Section
Ambient Geochemistry/ Geochemical Conditions	1.2	2.1
Repository Conditions	1.2.5	2.2
Temperature	*1.2.5.2*	*2.1*
Humidity	*1.2.5.3*	*2.1*
Water Content	*1.2.5.3*	*2.1*
Pressure	*1.2.5.1*	*2.1*
Brine Volume	*1.2.5.4*	*2.1*
Waste Characteristics / Inventory	1.2.3	3.1
Gas Phase / Production	2.1	4.1
Microbial Activity	2.1.5	4.2
radiolysis	2.1.7	3.4
Dissolution and Dissociation Terms	4.2.1	6.5.
Table Am	4.3.1.1	6.5.1
Colloids	5	3.5
Actinide Source Term	4	6

Information Only

GEOCHEM-9.2 Chammi Miller Appendix Geochem 2024 outline

1	Introduction and conceptual model
2	Repository Chemistry Process Models
	Map – Appendix Geochem, SOTERM and Leigh list
3	Baseline solubility
4	Uncertainty analysis
5	Gas Generation and Metal Corrosion
6	Colloid enhanced solubility
	Constructive criticism

Repository Chemistry Process Models subtopics.

1. Basic Thermodynamic Model Major Ions and Minerals
2. Thermodynamic Sub-model for MgO
3. Sub-model for Iron Species
4. Sub-model for Lead Species
5. Thermodynamic Sub-model for Organic Ligands
6. Summary of thermodynamic sub model for Actinide
7. ~~Thermodynamic Sub-model for An(III)~~
8. ~~Thermodynamic Sub-model for An(IV)~~
9. ~~Thermodynamic Sub-model for An(V)~~
10. Sub-model for Borate Species
11. Sub-model for Sulfide Species

Information Only